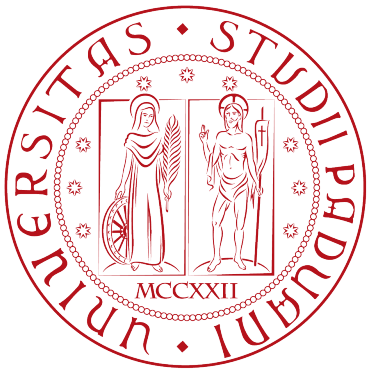

UNIVERSITÀ DEGLI STUDI DI PADOVA

Dipartimento di MEDICINA MOLECOLARE

CORSO DI DOTTORATO DI RICERCA: MEDICINA MOLECOLARE

CICLO XXXI

YAP/TAZ regulate autophagy to support epithelial plasticity and cancer stemness

Coordinatore: Ch.mo Prof. Stefano Piccolo

Supervisore: Ch.mo Prof. Stefano Piccolo

Dottorando: Qiuyu Zhuang

INDEX

The work presented in this thesis was supervised by Prof. Stefano Piccolo and co-supervised by Dr. Antonio Totaro, to whom goes my sincere gratitude for outstanding day to day mentorship and support.

Contributions to our work were given by: Dr. Tito Panciera, Dr. Daniele Di Biagio and Dr. Giusy Battilana. Great thanks also to Prof. Michelangelo Cordenonsi, for invaluable advice and co-supervision and for helping me in bioinformatic analyses.

ABSTRACT (ENGLISH)

YAP and TAZ play a fundamental role in oncogenic transformation, organ development, stem cell amplification and regeneration during tissue damage. YAP and TAZ elicit their biological functions through the transcriptional regulation of downstream genes and effector pathways. We found that autophagy is modulated by YAP and TAZ. Given the central role of YAP and TAZ in mechanotransduction, we also confirmed that the mechanical cues control autophagy through YAP/TAZ. Importantly, autophagy control is integral to YAP/TAZ biology.

ABSTRACT (ITALIAN)

YAP e TAZ sono dei coattivatori trascrizionali che giocano un ruolo fondamentale nella trasformazione oncogenica, nello sviluppo degli organi e nel preservare la capacita' dei tessuti di riparare le ferite. In parte queste funzioni sono il prodotto del ruolo di YAP/TAZ come stimolatori della generazione di nuove cellule staminali in condizioni di danno tissutale. YAP/TAZ agiscono attraverso la regolazione trascrizionale, a valle, di geni bersaglio e di vie effettrici. In questo studi abbiamo scoperto che YAP/TAZ controllano il flusso autofagico. Dato il ruolo centrale di YAP/TAZ in meccanotrasduzione, abbiamo verificato come la meccanotrasduzione sia un determinante chiave nei flussi autofagici delle cellule. Concludiamo che il controllo dell'autofagia e' integrale alla biologia di YAP/TAZ.

EXTENDED ABSTRACT

INTRODUCTION. YAP and TAZ (YAP/TAZ), two highly related transcriptional co-activators, recently emerged as fundamental sensors by which cells read structural and architectural features of their environment through mechanotransduction. By integrating biomechanical signals with other environmental cues, such as growth factor signalling and nutrient availability, YAP/TAZ transcriptionally control cell fates. A critical function of YAP/TAZ is the capacity to induce cell plasticity, including conversion of non-stem cells into stem-like cells.

HYPOTHESIS AIM OF THE THESIS. We hypothesized that YAP/TAZ might regulate autophagy in mammary epithelial cells. Autophagy is a catabolic process by which intracellular structures and organelles are degraded and recycled in the cell.

We asked whether YAP/TAZ require an increased autophagic flux to support the metabolic demands of YAP/TAZ-driven cell proliferation and as a means to induce cytoplasmic remodeling, an essential feature of YAP/TAZ driven phenotypic plasticity. Given the central role of YAP/TAZ in mechanotransduction, we also investigated the possible mechanical regulation of autophagy through YAP/TAZ.

RESULTS AND DISCUSSION. We found that YAP/TAZ control the cell's autophagic flux by regulating the fusion of autophagosomes with lysosomes. Challenging cells with different mechanical signals reflects into biomechanical regulation of autophagy. YAP/TAZ promote autophagy through the transcriptional regulation of the TBC1D2 gene. Autophagy is a critical process to sustain oncogenic traits and cancer stem cell properties, and to promote cell plasticity and self-renewal of somatic SCs through YAP/TAZ.

In general, our work uncovered a novel function of YAP/TAZ in regulating autophagy, suggesting that autophagy serves as a key downstream effector of YAP/TAZ biological functions.

INTRODUCTION

YAP/TAZ upstream and downstream regulation

Yes-associated protein (YAP) and transcriptional co-activator with PDZ-binding motif (TAZ) are two major transcriptional regulators in modulating tissue homeostasis, organ size, regeneration and tumorigenesis. Accumulating evidence shows that YAP/TAZ activation is widespread in many human tumors (Zanconato, Cordenonsi, & Piccolo, 2016). Due to these pioneering discoveries, increasing attention has been paid to the study of YAP/TAZ and their related biology.

Hippo signalling and YAP/TAZ

The Hippo signalling cascade has emerged at the center in controlling YAP/TAZ activities. The four core components that constitute Hippo signal transduction kinase cascade were first discovered in *Drosophila* as tumor suppressor genes: the protein kinase Hippo (Hpo) and its partner Salvador (Sav), the NDR family protein kinase Warts (Wts) and its adaptor protein Mob-as-tumor-suppressor (Mats).
The detailed mechanisms of this pathway have been well described: when activated, Hpo and Sav phosphorylate Wts and Mats to induce Wts activation, then activated Wts subsequently phosphorylates the transcriptional co-activator Yorkie (Yki), leading to the accumulation of Yki in cytoplasm by interacting with 14-3-3. In contrast, when the pathway is inactivated, Yki is dephosphorylated and remains in an activated state, leading to a relocation in the nucleus to induce gene expression that related to survival and growth (Halder & Johnson, 2011). Because Yki does not have the DNA-binding activity, Yki controls gene expression of its targets by interacting with other factors such as Scalloped (Sd). Genetically, Yki overexpression or Hpo/Wts deficiency causes overgrowth of imaginal discs (Huang, Wu, Barrera, Matthews, & Pan, 2005).
The core Hippo signalling was identified as conserved in mammals: Hpo homologs MST1/2, Sav homolog SAV1, Wts homologs LATS1/2 and Mats homolog MOB1. The mechanism of the whole pathway is also very similar as in *Drosophila*. After binding to the regulatory protein SAV1/WW45, activated MST1/2 can

phosphorylate LATS1/2 and MOB1 for a stable LATS1/2-MOB1 complex. The activated LATS1/2-MOB1 complex then phosphorylates the Yki orthologs in mammalian YAP and TAZ, leading to their inactivation (Yu & Guan, 2013).

Biomechanical transduction and YAP/TAZ

Biomechanical transduction happens when cells sense the physical signals from the microenvironment and adjust themselves to the extracellular forces through a series of intracellular biochemical and biological reactions (Janmey & Miller, 2011). Accumulating evidence shows that mechanical inputs regulate YAP/TAZ activity to transfer the ex-cellular cues into gene expression to adjust to environmental changes. YAP/TAZ localization and activity are influenced by the extracellular matrix (ECM) stiffness, cell shape and the resulting cytoskeletal tension. When cells are plated on a stiff and/or unpatterned matrix (i.e., on a substrate on which cells can spread) YAP/TAZ localize predominantly inside the nucleus, where they exert their transcriptional activity. The localization is, instead, prevalently cytoplasmic when the adhesive substrate is soft or when cells are confined in a restricted area. In these conditions actin filamentous structures are not visible and YAP/TAZ, excluded from the nucleus, are not able to regulate gene expression. Furthermore, the relationship between cytoskeletal tension and YAP/TAZ regulation was also confirmed using specific drugs to impair the cytoskeletal functions (Dupont et al., 2011).

YAP/TAZ are proved to be key mediators of mechanical signals and their potent biological effects (proliferation, survival, differentiation). For example, endothelial cells die when forced to remain small, whereas they proliferate when they are allowed to spread, and YAP/TAZ dictate these opposite behaviors (Dupont et al., 2011). In addition, YAP/TAZ regulation by cell shape and rigidity of ECM dictates a pivotal stem cell decision: to remain undifferentiated and grow, or to activate a terminal differentiation program (Totaro et al., 2017).

The detailed mechanisms of YAP/TAZ regulation by mechanical inputs are only partially understood. ECM regulation on YAP/TAZ is F-actin cytoskeleton dependent: modulating F-actin organization through capping and severing proteins such as Cofilin-1 and CapZ changes the cytoskeletal tension and then ultimately regulates YAP/TAZ activity (Aragona et al., 2013). Consistent with the idea that

YAP/TAZ activity is connected to the tensile status of the F-actin cytoskeleton, components of focal adhesions (FAs), focal adhesion kinase (FAK) and Src are also reported to be mediating factors of YAP/TAZ (Martin et al., 2016).

Other upstream signalling

YAP/TAZ are reported to be components of the destruction complex in Wnt pathway and required for β-catenin regulation. In turn, Wnt ligands also control YAP/TAZ nuclear localization through destruction complex to switch on Wnt-induced, YAP/TAZ-dependent transcriptional responses (Azzolin et al., 2014).
YAP/TAZ activity can also be regulated by metabolic homeostasis, GPCR signalling, inflammatory signalling and other signalling pathway (reviewed in Totaro, Panciera, & Piccolo, 2018).

Nuclear YAP/TAZ biology

When the Hippo signalling or the other upstream signalling is inactive and YAP/TAZ are de-phosphorylated, YAP/TAZ are switched to an activated state. YAP has five serine/threonine phosphorylation residues (S61, S109, S127, S164, S381 for human YAP) and TAZ has four (S66, S89, S117, S311 for human TAZ). S127 for YAP and S89 for TAZ are the most important sites among these residues for YAP/TAZ activities, as after being phosphorylated at S127 or S89 respectively, YAP/TAZ interact with 14-3-3 and remain in the cytoplasm, losing the ability to translocate in the nucleus to activate downstream targets. Thus, constructs bearing all serine to alanine mutations (YAP-5SA and TAZ-4SA) or mutation at S127 for YAP (S89 for TAZ) are most widely used as the constitutive active form for YAP/TAZ (Zhao, Li, Lei, & Guan, 2010).
After being dephosphorylated, YAP/TAZ nuclear localization increases and YAP/TAZ can activate target gene transcription.
YAP/TAZ cannot bind DNA-directly; rather, they can only serve as transcriptional co-activators and require DNA-binding factors, such as p73, Runx2, PPAR- γ, et al., to exert transcriptional functions. Among all these DNA-binding factors, the TEA-domain family members TEAD1/2/3/4 serve as the main DNA binding platform to which YAP/TAZ associate on target enhancers and promoters. TEADs

support most, if not all, what we know about YAP/TAZ-driven gene transcription and biology (Zhao et al., 2008). Motif analyses at YAP/TAZ peaks through ChIP-seq revealed that TEAD proteins are the major platforms for YAP/TAZ interaction with DNA. Collectively, YAP/TAZ/TEAD complex binds to DNA at the genome-wide level to regulate YAP/TAZ-dependent proliferation and survival profiles majorly by controlling the expression of genes involved in cell cycle, such as cyclins and their regulators, mitosis regulators and also genes regulating DNA replication and repair. Moreover, it has been recently reported that YAP/TAZ/TEAD form a complex with another transcriptional factor, AP-1 (the dimer between Jun and Fos family members). YAP/TAZ/TEAD and AP-1 synergistically activates >70% of all YAP/TAZ target genes, including a variety of genes directly involved in the control of S-phase entry and mitosis (Croci et al., 2017; Totaro et al., 2018; Zanconato et al., 2015).

YAP/TAZ biological functions

YAP/TAZ and organ growth

The important role of YAP/TAZ in organ growth has been proved in knockouts and conditional knockout alleles in both *Drosophila* and mammalian models. In *Drosophila*, the loss of Hippo pathway or the transgenic overexpression of Yki (the YAP gene in flies) causes overgrowth of organs such as eyes, wings, or other appendages (Dong et al., 2007).

Similarly, this pathway is conserved also in mammals: In mouse liver, transgenic overexpression of YAP or liver-specific knockout of Mst1/2 or Sav1 all cause organ enlargement and hyperplasia (Camargo et al., 2007; Lee et al., 2010; Zhou et al., 2009). In mouse heart, Sav1, Mst1/2 or Lats2 conditional knockout or transgenic YAP overexpression leads to hearts enlargement and thickened myocardium (von Gise et al., 2012). Consistent results were obtained in other tissues for example pancreas and intestine, where transgenic overexpression of YAP induces cell proliferation and impairs differentiation (Camargo et al., 2007).

YAP/TAZ and tumorigenesis

Consistent with the important role of the Hippo pathway in tissue growth, loss of function in Hippo signalling components has been linked to tumorigenesis. For instance, MST1/2, MOB1 or LATS1/2 inactivation leads to different human cancers in respective tissues. As the most important effectors of the Hippo signalling, YAP/TAZ also serve as tumor promoters. It has been characterized that YAP/TAZ are highly activated in different tumor samples (Piccolo, Dupont, & Cordenonsi, 2014). Moreover, YAP has been identified as an oncogene in human hepatocellular carcinomas, in breast cancers, and other cancers (Zanconato et al., 2016). YAP/TAZ-dependent oncogenic traits mostly rely on their capacity to promote aberrant cell proliferation, induce epithelial-to-mesenchymal transition (EMT) and sustain chemoresistance (Mo, Park, & Guan, 2014).

YAP/TAZ and stem cell

Increasing evidence suggests that the contribution of YAP/TAZ in organ growth and cancer are related with the regulation of stem cells self-renewal and expansion capacities. YAP/TAZ are essential for the regulation of tissue-specific progenitor cells. YAP expression is majorly restricted in progenitor/stem cells in normal intestine tissues, and transgenic activation of YAP *in vivo* expands the undifferentiated progenitor cells in different tissues (Camargo et al., 2007; Cao, Pfaff, & Gage, 2008). Consistent with the *in vivo* data, transient expression of YAP/TAZ *ex vivo* can convert differentiated cells from different tissues including mammary glands, neurons and pancreas into the tissue-specific stem/progenitor cells (Panciera, Azzolin, Fujimura, Di Biagio, et al., 2016).

YAP and TAZ have also been indicated to be important for cancer stem cells (CSCs) in malignant glioma and breast cancer. It was reported that TAZ is required for the tumor-initiation capacities of breast cancer cells, as TAZ gain of function drives non-cancer-stem cells population to cells with tumor-initiating and self-renewal abilities and loss of TAZ impairs this capacity in CSCs-enriched populations (Cordenonsi et al., 2011). In parallel, loss of TAZ impairs invasiveness, self-renewal and tumorigenic potential also in primary glioblastoma stem cells (Bhat et al., 2011).

Autophagy

Autophagy, or self-eating, is a catabolic process where organelles and macromolecules are sequestrated and transported to lysosomes for degradation. The degradation products can then be recycled and replenish the cell with nutrients or building materials (Mizushima, 2007). Autophagy is a conserved and fundamental process. At basal levels, this process contributes to the preservation of cellular fidelity and maintenance of cellular homeostasis. Autophagy can also be activated by various stresses for example limited nutrients or oxygen, dysfunctional components and microbe invasion, which acts as a survival mechanism to help the cells adjust to the environmental changes (Khaminets, Behl, & Dikic, 2016).

The molecular machinery of autophagy

Autophagy starts from the formation of a crescent-shaped, double-membraned structure, called phagophore (See Introductory Figure here below). This highly regulated process involves two major kinases, the UNC-51-like kinase (ULK) and the Class III phosphatidylinositol 3-kinase (Class III PI3K) VPS34, together with their associated regulatory factors and autophagy-related (ATG) proteins. Then phagophore elongates and subsequently encloses a portion of cytoplasm, which results in the formation of the autophagosome. Phagophore elongation and autophagosomes formation require the incorporation of phosphatidylethanolamine-lipidated LC3 which serves as a cargo receptor to identify and deliver misfolded or aggregated proteins, fragments of the endoplasmic reticulum and damaged organelles to the autophagosome for degradation. Two ubiquitin-like protein conjugation systems composed of multiple ATG proteins such as ATG5 and ATG7 are also involved in conjugating phosphatidylethanolamine to LC3. Eventually, the outer membrane of the autophagosome fuses with the lysosome into an autolysosome, where the resident lysosomal hydrolases degrade the enclosed materials together with the inter membrane of the autolysosome (Introductory Figure). Amino acids and other small molecules that are generated by autophagic degradation are then delivered back to the cytoplasm for recycling or energy production (reviewed in Mizushima, Yoshimori, & Levine, 2010).

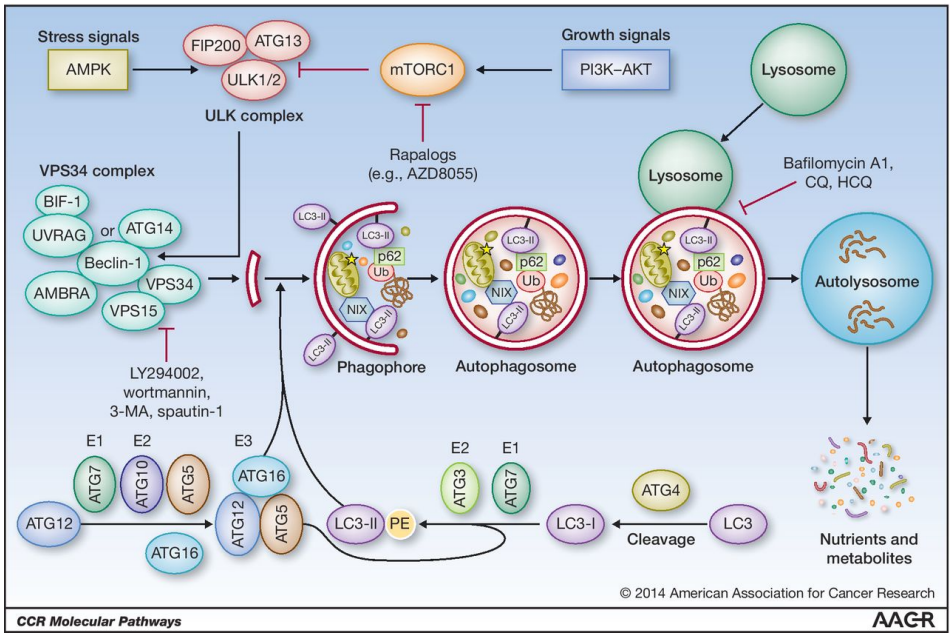

Introductory Figure: The process of autophagy. Schematic representation of the main steps, molecular players and pharmacological modulators of the autophagy process. See the main text for more details. Abbreviation: 3-MA, 3-Methyladenine; ATG, autophagy-related gene; CQ, chloroquine; LC3: microtubule associated protein 1 light chain 3; PE: phosphatidylethanolamine; ULK: the UNC-51-like kinase; VPS: vacuolar protein sorting. Adapted from Cicchini, Karantza, & Xia, 2015.

Autophagy and cancer

In cancer cells autophagy fulfils a dual role, having both tumor-suppressive and tumor-enhancing properties. The first support of autophagy as a tumor suppressor came from the study of the autophagy gene BECN1. BECN1 depletion was reported to be associated with several human cancers and heterozygous deletion of Becn1 in mice increases the incidence of spontaneous tumors. (Liang et al., 1999; Yue, Jin, Yang, Levine, & Heintz, 2003). In addition, several ATG genes mutations are found in gastric and colorectal cancers and mice lacking ATG5 or ATG7 develop benign liver adenomas (Kang et al., 2009; Takamura et al., 2011).

On the other hand, increasing evidence also indicates that tumor cells require autophagy for their survival. Elevated activation of autophagy and accumulation of

autophagosomes are found in tumor regions, at least suggesting that tumor cells exploit abnormally high level of autophagy (Mizushima, 2009).

Tumors cells are usually affected with multiple stresses including starvation, growth factor deprivation and hypoxia. Thus, autophagy-mediated intracellular recycling is able to provide fresh nutrients and energy to meet the increasing metabolic demand in tumor regions (White, 2012). Intriguingly, oncogenic activation requires disproportional levels of autophagy to sustain tumor growth (Guo et al., 2011; Yang et al., 2011). These works suggest that autophagy supports the function of oncogenes to maintain homeostasis of aggressive cancers. The dominant interpretation of these results has been so far a metabolic one, that is, autophagy as a means to supply intracellular substrates and energy for growth. Besides, autophagy has been shown to sustain breast CSCs population, which provides another possible mechanism of autophagy to support tumorigenesis (Cufí et al., 2011).

Autophagy and stem cell

Stem cells are unique in their ability to self-renew and differentiate, which play an important role in development and tissue regeneration. Embryonic stem cells, for example, display an upregulation of autophagy level during early differentiation, which indirectly indicates the contribution of autophagy in stem cells (Tra et al., 2011). In the somatic stem cells, high autophagy activity is a general phenomenon of adult skin and blood stem cells, and autophagy inhibition in these cells largely impairs their self-renewal and differentiation capacities (Salemi, Yousefi, Constantinescu, Fey, & Simon, 2012). Furthermore, autophagy deficiency is able to abrogate OSKM induced reprogramming of fibroblasts into iPSCs (Ma et al., 2015; Wang et al., 2013).

Tools to study autophagy

To date, microtubule-associated protein light chain 3 (LC3) is the most widely-used marker for autophagosomes. Upon autophagy activation, the soluble form of LC3 known as LC3-I is subsequently conjugated with phosphatidylethanolamine (PE) to become LC3-II by a ubiquitination-like enzymatic reaction (Introductory Figure).

In contrast to the cytoplasmic localization of LC3-I, LC3-II associates with both the outer and inner membranes of the autophagosome (Tanida, Minematsu-Ikeguchi, Ueno, & Kominami, 2005). Different isoforms of LC3 protein levels can be detected through immunoblotting: although the molecular weight of LC3-II is larger than that of LC3-I due to the addition of PE, LC3-II migrates faster than LC3-I in SDS-PAGE probably because of its extreme hydrophobicity. Thus, endogenous LC3 is detected as two bands, and the lower band which represents LC3-II serves as an indicator of autophagosome formation (Mizushima & Yoshimori, 2007). Since the dynamic range of LC3 immunoblots is quite limited, it is imperative that other assays are used in parallel in order to draw valid conclusions about changes in autophagy activity. As an alternative assay, endogenous LC3 or LC3 fused with a fluorescent protein such as GFP (GFP-LC3) has been used to monitor autophagy through indirect immunofluorescence or direct fluorescence microscopy. In this case, LC3 can be visualized either as a diffuse cytoplasmic pool (LC3-I) or as punctate structures (LC3-II) that represent autophagosomes (Mizushima et al., 2010).

To fully understand a given biological process, it is usually critical to perform experiments to modulate the activity of the process. One of the most serious problems in current autophagy research is that we still lack highly specific autophagy inhibitors and activators. Nonetheless, several pharmacological modulators and genetic manipulation techniques are now available. As Class III PI3K is largely required for autophagosome formation, one of the widely used pharmacological approaches to impair autophagy in vitro is the use of PI3K inhibitors such as wortmannin, LY294002, or 3-MA (Introductory Figure). Other major pharmacological inhibitors such as chloroquine, bafilomycin A and pepstatin A target the later steps of autophagy by blocking the final degradation of autophagic cargo inside autolysosomes (Klionsky et al., 2016) (Introductory Figure).

However, it should be noted that these reagents may affect other cellular processes besides autophagy. Thus, for a more valid conclusion, pharmacological studies should be combined with genetic approaches to more specifically inhibit the autophagy pathway. The most commonly used and efficient genes to be targeted (by siRNA, CRISPR or genetic knockout) include ATG3, ATG5, BECN1, ATG7 and FIP2000. In general, a combination of different pharmacological and genetic

approaches that act at different steps in the autophagy is advised during studies (Mizushima et al., 2010).

AIMS AND WORKING HYPOTHESES

YAP/TAZ play a fundamental role in oncogenic transformation, tissue regeneration and organ growth. YAP/TAZ operate as transcriptional coactivators and recent work is starting to shed light on their vast repertoire of target genes. Only in part the biological functions of YAP/TAZ can be ascribed to the broad number of YAP/TAZ target genes involved in cell proliferation. YAP/TAZ indeed control cell phenotypic plasticity, inducing stemness properties independently from proliferation. As such, the mechanisms underpinning their biological effects still remain largely enigmatic.

Autophagy is a catabolic process by which intracellular structures and organelles are degraded and recycled in the cell. Autophagy is also essential for the remodelling of the intracellular structures and the reprogramming of cellular metabolism associated with cancer progression and cell plasticity. Considering the crucial role of YAP/TAZ in these processes, we wondered if autophagy and YAP/TAZ biology may be in fact connected.

Here we first tested the relevance of YAP/TAZ to regulate autophagy in mammary epithelial cells. Secondly, given the central role of YAP/TAZ in mechanotransduction, we verified whether mechanical signals regulate autophagy through YAP/TAZ. We further performed experiments to identify the specific target(s) by which YAP/TAZ regulate autophagy levels. Lastly, we validated that YAP/TAZ require autophagy to sustain oncogenic traits, cancer stem cell properties, and, in normal cells, cell plasticity and stem cells' self renewal.

RESULTS

YAP and TAZ control autophagic flux in mammary epithelial cells by regulating the fusion of autophagosomes with lysosomes

We started this work by assessing whether YAP and TAZ (YAP/TAZ) could be involved in the regulation of the autophagic flux. To this aim, we knocked down both the YAP and TAZ mRNA with two independent siRNA mixes (siYAP/TAZ #1 and siYAP/TAZ #2) in MDA-MB-231 triple-negative breast cancer (TNBC) cells. First, we confirmed the siRNAs downregulation efficiency 48 hours after transfection by immunoblot. Both siYAP/TAZ #1 and siYAP/TAZ #2 siRNA mixes efficiently decreased the expression of the endogenous YAP and TAZ proteins (Fig. 1A). We next evaluated the effects of YAP/TAZ downregulation on autophagy by monitoring the protein levels of phosphatidylethanolamine-conjugated form of LC3 (LC3-II), an established marker of autophagosome formation. We found that knockdown of YAP/TAZ led to an increase in LC3-II protein levels in mammary MDA-MB-231 cells (Fig. 1A). To evaluate the generality of this finding, we extended our analysis to the non-transformed MCF10A mammary epithelial cells. As shown in Fig. 1B, we confirmed an increase in LC3-II protein levels upon YAP/TAZ knockdown also in MCF10A cells.

To further confirm these data, we monitored autophagy levels through fluorescence microscopy by following the GFP fluorescent signal in cells expressing the LC3 protein fused at its N terminal with a GFP tag (GFP-LC3). To this end, we generated a MDA-MB-231 cell lines stably expressing GFP-LC3, hereafter referred to as MDA-MB-231-GFP-LC3. Consistent with LC3-II accumulation shown in Fig. 1A, we observed an accumulation of autophagosomes upon YAP/TAZ knockdown with two independent siRNA mixes, as indicated by the increase in the area of the cell occupied by GFP-LC3 puncta (Fig. 1C-D). As accumulation of GFP-LC3 puncta could be attributed to either an increase of the autophagy induction or an impaired autophagosome turnover, we analyzed the effect of YAP/TAZ knockdown on autophagic flux also in the presence of chloroquine (CQ), an inhibitor of autophagosomes degradation. The rationale of this experiment is the following: if the GFP-LC3 puncta accumulation observed upon YAP/TAZ knockdown is due to

an increase of autophagy induction, YAP/TAZ downregulation should still induce in CQ-treated cells more GFP-LC3 puncta compared to the control siRNA transfected cells. On the other hand, if YAP/TAZ knockdown blocks the late steps of autophagosome degradation, CQ-induced autophagosome accumulation should be already at plateau, and thus no differences should be observed in the level of GFP-LC3 puncta compared to the control siRNA cells in these conditions. As shown in Figure 1C-D, upon CQ treatment, the second scenario turned out true, as we observed an increase of GFP-LC3 puncta in both control and YAP/TAZ knockdown cells, but YAP/TAZ knockdown did not cause a further accumulation of GFP-LC3 puncta compared to control cells (Fig. 1C-D). The same results were obtained with the Ras-transformed MCF10A-T1k (MII) cell line, an isogenic derivative of the MCF10A mammary cell line. Indeed, we found that MII cells stably expressing the GFP-LC3 construct, hereafter called MII-GFP-LC3, show an accumulation of GFP-LC3 puncta upon YAP/TAZ depletion by siRNA transfection, while this difference is lost upon CQ treatment (Fig. 1E-F). Taken together, all the evidence indicates that YAP/TAZ knockdown leads to autophagosome accumulation by impairing the late steps of autophagosome turnover rather than enhancing the formation of autophagosomes.

Since the data indicate that YAP/TAZ knockdown might impair the late steps of autophagosome turnover, we looked at the fusion step of autophagosomes with lysosomes. We analyzed the distribution of these two intracellular structures in MDA-MB-231-GFP-LC3 cells, visualized through the GFP-LC3 fluorescent signal of autophagosomes and the staining for the lysosomal-associated membrane protein 1 (LAMP1), as a marker for lysosomes. In control siRNA transfected cells, we observed an extended colocalization between the GFP-LC3 puncta and the LAMP1 staining, indicating a successful generation of autolysosomes structures (yellow) from the fusion of autophagosomes (green) with lysosomes (red) (Fig. 1G-H). On the other hand, YAP/TAZ knockdown induced a reduction in the colocalization between GFP-LC3 puncta and LAMP1 staining, compared to the control cells, suggesting an impairment in the fusion of autophagosomes with lysosomes (Fig. 1G-H).

Taken together, these data indicate that YAP/TAZ regulate the late step of autophagic flux in mammary epithelial cells, by controlling autolysosome formation.

YAP/TAZ control of the autophagic flux depends on their transcriptional activity

Since YAP/TAZ sustain their biological functions mainly by regulating gene transcription, we next validate whether their role in the regulation of autophagy relies on their transcriptional activity. For this, MII-GFP-LC3 were transduced with either an empty lentiviral vector (Empty) or with doxycycline-inducible lentiviral vector encoding a siRNA-insensitive YAP *wild-type* (YAP WT) construct. We also used a YAP mutant carrying the S94A mutation, disabling any interaction with TEAD, the main YAP/TAZ-binding platform on DNA (YAP S94A). We knocked down endogenous YAP/TAZ by siRNA transfection in the lentiviral transduced MII-GFP-LC3 cells and treated cells with doxycycline to induce ectopic YAP expression. At 48 hours after siRNA transfection, cells were fixed and analyzed by fluorescence microscopy for GFP-LC3 puncta. As shown in Fig. 2A-B, we confirmed the accumulation of GFP-LC3 puncta in the Empty-control cells upon YAP/TAZ depletion by siRNA transfection, in absence of CQ. However, the expression of YAP WT, but not of YAP S94A, was sufficient to prevent GFP-LC3 puncta accumulation upon YAP/TAZ knockdown, confirming the specificity of the observed effects with our siRNA knockdown reagents. In the same vein, upon CQ treatment, we observed an increase of GFP-LC3 puncta in all the experimental conditions, but no statistical differences were observed upon either YAP/TAZ knockdown or YAP overexpression, confirming in such "add back" experimental setting that YAP/TAZ control the autophagic flux by regulating the late steps of autophagosome turnover (Fig. 2A-B).

As control for these experiments, YAP/TAZ transcriptional activity was monitored by the quantitative PCR with reverse transcription (qRT–PCR) analysis of mRNA levels for the YAP/TAZ-target gene CTGF. Indeed, we confirmed the inhibition of the YAP/TAZ transcriptional activity in the Empty-control cells upon YAP/TAZ siRNA transfection. Moreover, the concomitant overexpression of a siRNA-insensitive YAP WT construct, but not the YAP S94A mutant, was able to rescue the YAP/TAZ transcriptional activity as indicated by the recovery of the mRNA levels for CTGF (Fig. 2C).

YAP/TAZ mechanotransduction regulates autophagy

YAP/TAZ activity is regulated by the mechanical cues instructed by the cellular and tissue microenvironment and transmitted across the cell through the actomyosin structures of the cytoskeleton (Totaro et al., 2018). Thus, we investigated if mechanical signals could affect autophagy through the regulation of YAP/TAZ. First, we investigated mechanical stimuli conveyed from extracellular matrix (ECM) coated substrates at different degrees of stiffness. For this, we plated MII-GFP-LC3 cells on soft vs. stiff fibronectin-coated acrylamide hydrogels of 2.0 kPa vs. glass, respectively. Indeed, in our laboratory we previously demonstrated that the mechanoresponse of cells plated on stiff hydrogels above 4kPa was undistinguishable from that of cells plated on plastic or glass (Dupont et al., 2011; Totaro et al., 2017). Thus, for simplicity, and after preliminary pilot studies in which we found no difference in autophagic flux between the rigidity of glass and that one of 40kPa, we used fibronectin-coated coverslips to mimic "stiff" substrates. MII-GFP-LC3 cells plated on the indicated substrates were let adhere and grow for 24 hours and treated with or without CQ for the last 4 hours. Finally, the cells were fixed and analyzed by fluorescence microscopy to assess autophagy activity. When plated on soft hydrogels, where YAP/TAZ are inactive (Dupont et al., 2011), we observed an increase in the number of cells accumulating GFP-LC3 puncta, compared to cells plated on stiff, recapitulating the effects of YAP/TAZ knockdown (Fig. 3A-B). As control, CQ treatment caused, as expected, an increase in GFP-LC3 puncta in MII-GFP-LC3 cells plated on both stiff and soft substrates, but no significant difference was observed in the number of GFP-positive cells between the two conditions (Fig. 3A-B), paralleling YAP/TAZ regulation.

We also looked at the YAP and TAZ subcellular localization, as a reliable indicator of their transcriptional activity. We confirmed that YAP/TAZ were predominantly cytoplasmic (inactive) in MII-GFP-LC3 cells plated on soft, while they were mainly nuclear (active) in cells plated on stiff substrate, suggesting a correlation between the regulation of autophagy flux and YAP/TAZ activity dictated by soft ECM (Fig. 3A-C).

To demonstrate that the impairment of the autophagic flux induced by a soft ECM depends on the inhibition of YAP/TAZ, we investigated whether raising YAP/TAZ activity in soft-plated cells is sufficient to rescue autophagy. To this end, MII-GFP-

LC3 cells infected with either an empty vector (Empty) or with doxycycline-inducible lentiviral vectors encoding for the YAP WT and YAP S94A constructs. Upon YAP WT overexpression, we observed a reduction in the number of cells accumulating GFP-LC3 puncta compared to the Empty-infected control condition, all in cells plated in soft ECM (Fig. 3D). On the other hand, the transcriptionally inactive YAP S94A mutant was unable to prevent LC3-II accumulation in M2-GFP-LC3 plated on soft hydrogel, confirming that YAP/TAZ control autophagy through their transcriptional activity (Fig. 3D).

High cell density in postconfluent epithelial monolayers is another condition known to turn-off YAP/TAZ activity through attenuation of cellular mechanotransduction (Totaro et al., 2018). Accordingly, MII-GFP-LC3 cells were plated for 24 hours at low- or high-density respectively, and then analyzed by fluorescence microscopy to assess autophagy activity. We observed that, in analogy with cells plated on soft hydrogel, the high-density (Dense) condition induced accumulation of GFP-LC3 puncta compared to cells plated at low-density (Sparse) (Fig. 3E-F). Furthermore, the overexpression of YAP in MII-GFP-LC3 cells plated at high density is able to prevent autophagosome accumulation, as indicated by the reduction of the area of GFP-LC3 puncta per cell compared to the control MII-GFP-LC3 plated at the same cellular density (Fig. 3E-F). Finally, CQ treatment caused an accumulation of GFP-LC3 puncta in MII-GFP-LC3 plated either at low or high density, but no significant difference was observed between the two conditions when lysosomal degradation was inhibited (Fig. 3E-F).

The mechanical properties of the extracellular microenvironment are transduced inside the cells mainly by the structural organization and the tension of the actomyosin cytoskeleton, which senses and adapts itself in response to mechanical signals from the outside. Thus, we reasoned to mimic a low tension-dictating microenvironment by impairing cytoskeletal functions with specific drugs, such as Latrunculin A (LatA), that disrupts cytoskeletal integrity by sequestering monomeric globular actin, and the inhibitor of the myosin light chain kinase ML-7, that impairs actomyosin contractility.

Hence, MII-GFP-LC3 cells were treated either with vehicle or LatA for 24 hours, incubated with or without CQ for the last 4 hours and analyzed by fluorescence microscopy to evaluate autophagy activity. The quantification of the area occupied by GFP-LC3 puncta revealed that the disruption of the F-actin cytoskeleton induced

by LatA caused an accumulation of autophagosomes, compared to the vehicle-treated cells (Mock). On the other hand, CQ treatment caused an accumulation of GFP-LC3 puncta in MII-GFP-LC3 treated both without or with LatA, but no significant difference was observed between the two conditions (Fig. 4A-B). We observed consistent results when we blocked actomyosin contractility in MII-GFP-LC3 cells. Indeed, the ML-7 inhibitor induced a dose-dependent accumulation of the GFP-LC3 puncta compared to vehicle (Mock) treated cells (Fig. 4C-D).
Taken together these data indicate that lowering cell mechanics phenocopies the experimental turn off of YAP/TAZ activity, and impairs autophagic flux leading to the accumulation of GFP-LC3 positive autophagosome structures.

YAP/TAZ control autophagic flux through their direct target TBC1D2

In keeping with the notion that the control of the autophagic flux by YAP/TAZ relies on their transcriptional activity, we next tried to identify the YAP/TAZ target genes potentially involved in the regulation of autophagy. To this end, we generated a virtual YAP/TAZ chromatin "interactome map", listing the YAP/TAZ-regulated genes in MDA-MB-231 cells and the corresponding cis-regulatory elements that they bound (Zanconato et al., 2015) (See Methods and Material section for details). By searching this database for autophagy-related genes based on literature reports, we found several YAP/TAZ targets involved in the regulation of autophagy, including genes that encode for proteins regulating phagophore initiation (RHEB and NEDD4L), autophagosome formation (ATG3) and autophagosome/lysosome fusion (TBC1D2). Our attention was captured by the TBC1 domain family member 2 (TBC1D2) gene, which belongs to the large family of vesicle traffic coordinators RAB GTPases. TBC1D2 specifically interacts with LC3 protein at the level of autophagosome membranes and is involved in the formation and maturation of autophagic vesicles. Given our previous observation of an impairment in the fusion of autophagosomes with lysosomes upon YAP/TAZ depletion, we focused our analysis of YAP/TAZ-dependent autophagy regulating genes on TBC1D2 as our ideal candidate.
Based on our YAP/TAZ chromatin "interactome map", we found that YAP/TAZ interact with a TBC1D2-associated enhancer, located in the genomic region chr9:100,985,454-100,986,091. Thus, we first validated by chromatin

immunoprecipitation quantitative polymerase chain reaction (ChIP-qPCR) experiments that YAP/TAZ were specifically bound to this regulatory region. We used a YAP antibody to immunoprecipitate chromatin in both MDA-MB-231 and MII cells transfected with control or YAP/TAZ siRNA mixes, followed by qRT-PCR for the TBC1D2-associated enhancer or a cis-regulatory element of CYR61 as a positive control (Fig. 5A-B). We detected an enrichment of the TBC1D2-associated enhancer upon YAP-bound chromatin immunoprecipitation, that was lost upon YAP/TAZ knockdown (Fig. 5A-B). By qRT-PCR analysis we confirmed that expression of TBC1D2 depends on YAP/TAZ, since we observed a downregulation of TBC1D2 mRNA upon YAP/TAZ knockdown through three independent siRNA mixes (siYAP/TAZ #1, siYAP/TAZ #2 and siYAP/TAZ #3) in both MDA-MB-231 and MII cells (Fig. 5C-D). Moreover, the downregulation of TBC1D2 mRNA induced by YAP/TAZ siRNA transfection, was rescued by the siRNA-insensitive YAP WT construct, but not the YAP S94A mutant (Fig. 5E). These data collectively support the view that TBC1D2 is a direct transcriptional target of YAP/TAZ.

Next, we investigated whether TBC1D2 was involved in the regulation of the autophagic flux in mammary epithelial cells. First, we characterized by qRT-PCR three independent siRNAs against TBC1D2 (siTBC1D2 A, siTBC1D2 B and siTBC1D2 C), able to efficiently downregulate endogenous TBC1D2 mRNA (Fig. 6A). Then, we found by immunoblot that knockdown of TBC1D2 by two independent siRNAs led to an increase in LC3-II protein levels (Fig. 6B). We also evaluated the effects of TBC1D2 downregulation on autophagy through fluorescence microscopy in MII-GFP-LC3 cells. We found that knockdown of TBC1D2 by three independent siRNAs led to an increase in the area occupied by GFP-LC3 puncta per cells. Upon CQ treatment, we observed an increase of GFP-LC3 puncta in both control and TBC1D2 knockdown cells, but TBC1D2 knockdown did not cause a further accumulation of GFP-LC3 puncta compared to control cells, in keeping with the model that TBC1D2 regulate a late step in autophagy (Fig. 6C-D). Collectively, these data indicate that TBC1D2 controls autophagic flux in mammary epithelial cells and its depletion recapitulate the effect on autophagy observed upon YAP/TAZ inhibition.

To understand if YAP/TAZ control autophagy through the transcriptional regulation of TBC1D2, we investigated if TBC1D2 is epistatic to YAP/TAZ in the regulation of autophagy. To this end, we knocked down either YAP/TAZ or TBC1D2 by siRNAs. At 48 hours after siRNA transfection, cells were fixed and analyzed by fluorescence microscopy for GFP-LC3 puncta. We observed GFP-LC3 puncta accumulation in Empty-control cells upon YAP/TAZ knockdown compared to the same cells transfected with control siRNA; however, this accumulation can be prevented by the overexpression the siRNA-insensitive YAP WT construct (Fig. 6E, compare frames a/b with d/e; Fig. 6F, compare lanes 1/2 with 4/5). Also importantly, YAP overexpression (by transduction of a doxycycline-inducible YAP lentiviral vector in MII-GFP-LC3), was unable to rescue the impairment of autophagic flux induced by TBC1D2 knockdown, as shown by the presence of GFP-LC3 puncta accumulation in YAP overexpressing cell transfected with TBC1D2 siRNA (Fig. 6E, compare frames a/c with d/f; Fig. 6F, compare lanes 1/3 with 4/6). Finally, CQ treatment induced GFP-LC3 puncta accumulation in all the experimental conditions, but no significant difference was observed among them (Fig. 6E; Fig. 6F, lanes 7-12). Thus, YAP overexpression can rescue autophagy inhibition after YAP/TAZ knockdown but not after TBC1D2 knockdown, indicating that TBC1D2 knockdown is downstream to YAP/TAZ in the regulation of autophagy.

Taken together these data indicate that YAP/TAZ promote autophagy through the transcriptional regulation of TBC1D2.

YAP/TAZ require autophagy to sustain oncogenic traits and CSC properties

Having established the involvement of YAP/TAZ in the regulation of autophagy, we next wondered whether autophagy contributes to the main YAP/TAZ biological functions as a downstream effector pathway. Given the relevance of YAP/TAZ for oncogenic proliferation, we first examined whether autophagy is required to promote the YAP/TAZ-dependent oncogenic traits. We used as model the MDA-MB-231 breast cancer cells, which have been previously characterized to be dependent on YAP/TAZ activity for their oncogenic features.

First, we evaluated the clonogenic growth of cancer cells upon inhibition of the autophagy pathway. To this end we transfected MDA-MB-231 with siRNA against

YAP/TAZ, or with either three independent siRNAs against TBC1D2 or a siRNA molecule targeting ATG7, a core component of the autophagic pathway that controls the early step of autophagosome formation. 24 hours after transfection, cells were trypsinized, seeded at the indicated clonogenic density and cultivated to allow colony formation. Seven days after replating, we observed that block of autophagy through the siRNA-mediated depletion of either ATG7 or TBC1D2 reduced the proliferation of MDA-MB-231 in clonogenic assay compared to the control siRNA transfected cells, recapitulating the effects of YAP/TAZ knockdown (Fig. 7A-B). To validate the generality of this finding, we also used two pharmacological inhibitors of autophagy: CQ, that block autophagosome/lysosome fusion, and 3-methyladenine (3-MA), that blocks the activity of the autophagy initiation complex. In agreement with the results obtained by siRNA-mediated depletion of ATG7 or TBC1D2, blocking autophagy by two different inhibitory drugs significantly reduced the growth of MDA-MB-231 cells in clonogenic assay, compared to vehicle-treated cells (Fig. 7A-B).

Next, we investigated the contribution of autophagy to the YAP/TAZ-dependent anchorage-independent growth of MDA-MB-231 cells, an additional trait of breast cancer malignant transformation. To this end, MDA-MB-231 cells were either transfected with different siRNA molecules or treated with pharmacological inhibitors of autophagy as previously described and plated on soft agar to assay their capacity to form and propagate as colonies. By monitoring the anchorage-independent growth in soft agar, we found that blocking autophagy by the mean of either TBC1D2- and ATG7-targeting siRNA molecules or pharmacological inhibitors recapitulates the effects of YAP/TAZ knockdown, strongly decreasing the number of colonies, compared to control-treated MDA-MB-231 cells (Fig. 7C-D).

The above finding led us to investigate if autophagy might be also required to sustain the YAP/TAZ-dependent cancer stem cells (CSCs) properties of breast cancer cells. To this aim, we performed a mammosphere assay with MII cells transduced with a TAZ construct carrying the constitutive activating S89A mutation (MII-TAZ S89A), that has been reported to confer CSC properties to benign MII breast cancer cells (Cordenonsi et al., 2011). The MII-TAZ S89A cells were either transfected with TBC1D2- or ATG7-targeting siRNA molecules or treated with the CQ or 3-MA autophagy inhibitors and replated after 24 hours in mammosphere-

forming growth conditions. As shown in Fig. 7E-F, either the siRNA-mediated depletion of ATG7 or TBC1D2 or the treatment with autophagy inhibitors CQ or 3-MA significantly reduced mammosphere formation of MII-TAZ S89A cells to the levels of the MII control cells transduced with an empty vector.
The data presented here show that YAP/TAZ require autophagy to sustain their dependent oncogenic traits and CSC properties in breast cancer cells.

Autophagy is critical for YAP/TAZ-dependent reprogramming and stemness maintenance: autophagy and generation of mammary stem cells by YAP

YAP/TAZ are essential regulators of cell behavior, including cell plasticity and self-renewing of somatic stem cells (SCs) during growth or in tissue repair and regeneration in adult tissues. It has been recently shown that transient activation of YAP or TAZ is able to convert ex-vivo terminally differentiated epithelial cells of different tissues, including mammary and pancreatic cells, into their corresponding tissue-specific progenitor cells (Panciera et al., 2016). Since cellular reprogramming and SC self-renewal require the activation of autophagy to induce remodeling of the intracellular structures and adjustment of metabolic program, we investigated the requirement of autophagy in the YAP/TAZ-mediated reprogramming and self-renewing of somatic SCs.
We used the mammary gland as a model system to validate whether autophagy is required for the YAP/TAZ-dependent reprogramming of the luminal differentiated cells (LD cells) into YAP-induced mammary gland stem cells (yMaSC), that are indistinguishable from the tissue resident mammary gland stem cells (MaSCs) (Panciera et al., 2016). To this end, we performed fluorescence-activated cell sorting (FASC) to purify LD cells which were then transduced with doxycycline-inducible lentiviral vectors encoding for YAP. Infected cells were treated with doxycycline to induce YAP-transgene expression, and contemporary treated with or without 3-MA. After seven days, cells were then plated at clonogenic density in three-dimensional 5% Matrigel cultures (see the diagram in Fig. 8A). Cells expressing YAP formed solid yMaSC colonies, while 3-MA treatment completely block YAP-induced colony formation (Fig. 8B-C), indicating that YAP/TAZ require autophagy to induce mammary gland reprogramming.

To determine whether autophagy was involved in YAP/TAZ-dependent self-renewal potential of yMaSCs, we dissociated YAP/TAZ-induced colonies from LD cells into single cells suspension and we replated them in colony condition with empty vehicle, CQ or 3-MA. We observed that pharmacological inhibition of autophagy by CQ or 3-MA completely blocked mammary colonies formation from single yMaSCs (Fig. 8D-E), indicating that YAP/TAZ require autophagy to sustain self-renewal in yMaSCs.

When expanded in specific culture conditions, yMaSC-derived colonies are able to undergo extensive budding and grow into large epithelial organoids that recapitulate in vitro mammary gland-like structures, similarly to the tissue-derived MaSCs. Thus, we validated the requirement of autophagy in YAP/TAZ-dependent regenerative potential of yMaSCs. For this, single cells from yMaSCs were cultured in organoid medium with empty vehicle, CQ or 3-MA. We observed that pharmacological inhibition of autophagy by CQ or 3-MA completely blocked mammary organoid formation (Fig. 8F-G), suggesting that autophagy is essential for YAP-dependent regenerative capacity of yMaSCs.

Autophagy is critical for YAP/TAZ-dependent reprogramming and stemness maintenance: autophagy and generation of amplifying pancreatic ductal cells by YAP

Next, we analyzed YAP-induced cell plasticity in pancreatic cells. Indeed it has been reported that also pancreatic exocrine acinar cells can be converted to progenitors by YAP overexpression, generating cyst-like organoids (or “yDucts”), morphologically and functionally indistinguishable from the pancreatic progenitors expanded in vitro as ductal organoids (Panciera et al., 2016).

We analyzed the autophagic flux in cultured yDucts and acinar cells grown in their corresponding media and treated for 4 hours with or without CQ. By immunoblot, we found that LC3-II protein levels were dramatically lower in yDucts compared to those of the acinar cells. However, the difference in the levels of LC3-II accumulation was dramatically reduced upon CQ treatment, suggesting a higher autophagy activity in YAP-induced yDuct pancreatic progenitors compared to the differentiated acinar cells (Fig. 9A). Thus, we investigated the effects of autophagy inhibition on YAP-induced reprogramming of acinar cells. Pancreatic acini from

R26-rtTA; tetO-YAP^{S127A} adult mice were isolated to obtain single pancreatic acinar cells preparation. Cells were plated in 100% Matrigel and cultured in pancreas organoid medium in the presence of doxycycline to induce YAP expression together with empty vehicle, CQ or 3-MA to determine the effects of autophagy inhibition (see the diagram in Fig. 9B). Acinar cells induced to express YAP, but not cells left without doxycycline, expanded as cyst-like organoids as described before. Remarkably, pharmacological inhibition of autophagy by CQ or 3-MA severely blocked YAP-induced organoid expansion (Fig. 9C-D), indicating that YAP/TAZ require autophagy to induce pancreatic acinar reprogramming.

We also verified the effects of autophagy impairment on YAP-dependent pancreatic self-renewal capacities. Single cells from yDuct were cultured with empty vehicle, CQ or 3-MA and analysed for their capacity to form cyst-like organoids. CQ and 3-MA completely abolished the self-renewal capacity in yDuct as no organoid was observed after 12 days of treatment (Fig. 9E-F). These results confirmed that autophagy is critical for YAP/TAZ-dependent stemness properties.

These data, together with the results obtained from the mammary gland reprogramming model, collectively suggest that autophagy is specifically required for YAP/TAZ-dependent reprogramming and self-renewal potential in different tissues.

DISCUSSION

Cell mechanics and its YAP/TAZ regulation impact autophagy

In this work, we characterized the role of YAP and TAZ in the regulation of the autophagy pathway. We found that YAP/TAZ control autophagy in epithelial cells through the transcriptional regulation of TBC1D2, which controls the fusion of autophagosomes with lysosomes. We also demonstrated that changes in the mechanical properties of the cells reflect into biomechanical regulation of autophagy through YAP/TAZ. YAP/TAZ play an essential role in oncogenic transformation, organ development and stem cell maintenance. Finally, we found that YAP/TAZ require autophagy to sustain oncogenic traits and cancer stem cell properties, and to promote cell plasticity and self-renewal of somatic SCs.

Autophagy is a highly dynamic process that can be modulated at several steps, including autophagosome formation and maturation, fusion with lysosomes to generate autolysosomes, and degradation. Through the use of both gain- and loss-of-function approaches, we found that YAP/TAZ control autophagic flux in different mammary cell lines, fostering autophagosome turnover through the regulation of the fusion between autophagosome and lysosomes vesicles.

YAP/TAZ are fundamental sensors by which cells read structural and architectural features of their environment through mechanotransduction. We demonstrated that turning off the YAP/TAZ activity, either by challenging cells with a low tension dictating microenvironment or by perturbing the actomyosin cytoskeleton, impairs autophagic flux. Several evidences reported that autophagy is activated in response to mechanical forces, to facilitate stress adaptation and remodel intracellular structures (King, 2012). However, the signalling pathways that mediate the mechanical induction of autophagy remained enigmatic. Our work fills this gap, as it indicates that YAP/TAZ serve as nexus to translate mechanical signals into biomechanical control of autophagy.

Transcriptional regulation of autophagy

Recent accumulating evidence has highlighted the importance of transcriptional regulation of autophagy to sustain prolonged autophagy and/or maintain basal autophagy (Baek & Kim, 2017; Sakamaki et al., 2017). By analyzing our list of YAP/TAZ direct targets in breast cancer cells, we noticed a number of autophagy-related genes that are potentially regulated by YAP/TAZ. These include genes that encode for proteins involved in phagophore initiation (RHEB and NEDD4L), autophagosome formation (ATG3) and autophagosome/lysosome fusion (TBC1D2). While our study indicates that TBC1D2 is the main mediator of YAP/TAZ in the regulation of autophagy in our model system, it's possible that additional YAP/TAZ targets can modulate autophagy at different level, based on cell or tissue type.

TBC1D2 belongs to the large family of TBCGAP, which coordinates the temporal-spatial activity of RAB GTPases. By controlling vesicle transport, the RAB GTPases integrate autophagy with intracellular trafficking and regulate different steps in autophagosome biogenesis (Kern, Dikic, & Behl, 2015). TBC1D2 interacts with membrane-bound LC3, where specifically inactivates Rab7 at the level of endosome and autophagosome vesicles. The impairment of TBC1D2 functions has been associated with the accumulation of enlarged autolysosomes and high levels of Rab7-GTP (Carroll et al., 2013; Toyofuku, Morimoto, Sasawatari, & Kumanogoh, 2015). We observed in our study that siRNA-mediated TBC1D2 depletion dramatically inhibits oncogenic traits and cancer stem cells (CSCs) properties in breast cancer cells. Although the molecular mechanisms by which TBC1D2 regulate autophagy have been described, our study for the first time suggests its functions in in tumor proliferation and malignancy.

Connecting autophagy to tumorigenesis

YAP/TAZ work as fundamental supervisors of both tissue repair mechanisms and tumor initiation/progression, given their ability to direct crucial cell functions, including proliferation, invasion, plasticity, survival and drug chemoresistance. In this study, we show that YAP/TAZ sustain their oncogenic traits by augmenting autophagic flux through their transcriptional activity. To start, we found that

autophagy inhibition by either genetic or pharmacological approaches impairs YAP/TAZ-dependent oncogenic growth and adhesion-independent transformation, the key attribute for YAP/TAZ in tumorigenesis. Moreover, we also revealed that autophagy is important for TAZ-induced CSCs expansion. Consistent with our study, accumulating evidence also suggests that autophagy plays a critical role in cancer biology. For instance, a study showed that deletion of FIP200, an important regulator of autophagy in mammalian cells, inhibits mammary tumorigenesis (Wei et al., 2011). Another study demonstrated that a key autophagy gene BECN1 are required for the tumorigenicity of breast cancer stem-like/progenitor cells (Yue et al., 2003). The underlying mechanism may relate to the catabolic capacity of autophagy and the metabolic shift in tumor cells. Autophagy recycles harmful or useless cellular components and replenishes the cell with fresh nutrients or building materials, which is important to support the increasing energy and synthetic demands during tumor initiation/progression (White, 2012).

Connecting autophagy to cellular reprogramming

Our study also proposes a novel role for autophagy in YAP/TAZ-dependent reprogramming from somatic cells to tissue-specific stem cells. The different metabolic states of somatic cells and progenitor cells may act as a roadblock for reprogramming. Compared with the normal maintenance of somatic cells, cellular reprogramming may have higher energy and nutrient demands for new cellular constructions and changes. Such metabolic demands may in turn activate autophagy to generate the building blocks for new cells. Notably, it has been reported that AMPK-mTOR signalling activates autophagy during iPSC reprogramming to meet the metabolic demands and that autophagy is crucial for establishing pluripotency (Ma et al., 2015; Wang et al., 2013). Evidence has also been provided by several groups that autophagy is required for self-renewal and differentiation of somatic stem cells (Nuschke et al., 2014; Salemi et al., 2012). These works are consistent with our conclusion, suggesting a novel but crucial role for autophagy in sustaining reprogramming.

That said, it is worth discussing whether YAP/TAZ induced autophagy may go well beyond the need to accompany reprogrammed cells in their potentially increased metabolic demands. We note that increased need of metabolites from autophagy

remains an assumption in many of the above studies. And that most of our observed effects occur in cells cultured in serum or anyway under saturating amounts of nutrients available from the cells' rich media. Moreover, YAP/TAZ activity does not necessarily increase cell proliferation; rather the primary event induced by YAP/TAZ is a change in gene expression accompanied to radical changes in cell structural, architectural morphology. Cell reprogramming indeed changes the cytoplasm, organelles and their organization in manners that must go hand in hand with changes in gene expression associated to changes in cellular states. Although so far sidestepped, the mechanisms coupling cell plasticity in the cytoplasm to those of the nucleus remains unknown. Here we propose that YAP/TAZ driven autophagy may represent one of such missing mechanism(s).

Modulation of autophagic activity is considered to be a potential therapeutic strategy for various diseases, including neuronal degeneration, infectious diseases and cancer (Puri & Chandra, 2014). Thus, identification of druggable autophagy regulators would be an attractive approach to treat these diseases. Although drugging YAP/TAZ is a challenging and ambitious goal for cancer research (Johnson & Halder, 2014), our findings that YAP/TAZ can regulate autophagy potentially provide new strategies for the clinical therapy against these diseases.

METHODS AND MATERIALS

Plasmids

pBABE-puro-GFP-LC3 construct was from Addgene (# 22405). pBABE-blasti-GFP-LC3 constructs were obtained by subcloning GFP-LC3 sequence from pBABE-puro-GFP-LC3 into pBABE-blasti-MCS backbone.
pBABE-hygro-FLAG-mTAZ S89A construct was described in Zanconato et al., 2015 and used for stable expression of TAZ variant in Fig. 7E-F.
cDNAs for siRNA-insensitive Flag-YAP WT and YAP S94A were subcloned into pCW57.1 doxycycline-inducible lentiviral vectors used for the experiments described in in Fig. 2, Fig. 3D-E, Fig. 5E and Fig. 6E-F. pCW57.1-MCS (empty vector) was used as control.
A different doxycycline-inducible lentiviral vectors-based strategy was used to induce the expression of YAP in the experiments described in Fig. 8B-C, Fig. 9C-D. cDNA for siRNA-insensitive Flag-YAP WT was subcloned in FUW-tetO-MCS backbone obtained by substituting the Oct4 sequence in FUW-tetO-hOct4 (Addgene #20726) with a new multiple cloning site (MCS). FUW-tetO-MCS (empty vector) or FUW-tetO-EGFP plasmids were used as controls.

Cell Cultures and reagents

MDA-MB-231 cells (from ICLC) were cultured in DMEM/F12 (Life Technologies) supplemented with 10% fetal bovine serum (FBS), glutamine and antibiotics.
MCF10A cells were from ATCC. MII cells were a gift from S. Santner (Santner et al., 2001). MCF10A and MII cells were cultured in DMEM/F12 with 5% horse serum (HS), glutamine and antibiotics, freshly supplemented with insulin, EGF, hydrocortisone, and cholera toxin.
HMEC cells were cultured in DMEM/F12 (Life Technologies) with bovine pituitary extract (BPE), glutamine and antibiotics, freshly supplemented with insulin, EGF, and hydrocortisone.

HEK293 cells (from ATCC) were cultured in DMEM (Life Technologies) supplemented with 10% FBS, glutamine and antibiotics. All cells are checked routinely for absence of mycoplasma contaminations.
To generate MDA-MB-231-GFP-LC3 cells, MDA-MB-231 cells were transduced with pBABE-puro-GFP-LC3 and were selected with puromycin. To generate MII-GFP-LC3 cells, MII cells were transduced with pBABE-blasti-GFP-LC3 and were selected with blasticidin.
Doxycycline hyclate, insulin, 3-methyladenine and chloroquine were from Sigma. Fibronectin and Lantrunculin A were from Santa Cruz Biotechnology. Murine EGF, murine bFGF, and human EGF were from Peprotech. B27 and BPE were from Life Technologies. Matrigel was from BD Biosciences (Corning). Rat tail collagen type I was from Cultrex.

Microfabrications and experimental settings

Fibronectin coated hydrogels of 2kPa elastic modulus were synthesized as previously described (Dupont et al., 2011; Totaro et al., 2017).
For experiments with hydrogels in 6 multi-well plates, cells were seeded in a 400ml drop on top of hydrogel; after attachment, the wells containing the hydrogels were filled with medium. For experiments with different cell densities, cells were plated at 10,000 cells cm^{-2} to obtain low-density cultures (sparse) or at 200,000 cells cm^{-2} to obtain monolayers at postconfluent cell density (dense).

RNA interference

siRNA transfections were done with Lipofectamine RNAi-MAX (Life technologies) in antibiotics-free medium according to manufacturer instructions. Sequences of siRNAs are provided in Table 1.
siYAP/TAZ #1 is composed of siYAP1 and siTAZ1 oligos; siYAP/TAZ #2 is composed of siYAP2 and siTAZ2 oligos; siYAP/TAZ #3 is composed of siYAP3 and siTAZ3 oligos. siYAP/TAZ refers to siYAP/TAZ #1 and siTBC1D2 refers to siTBC1D2 A if without specific mentioning.

Virus preparation

For lentivirus preparation, lentiviral particles were prepared by transiently transfecting HEK293T with lentiviral vectors together with packaging vectors pMD2-VSVG and pPAX2 by using TransIT-LT1 (Mirus Bio) according to manufacturer instructions. Briefly, 60µl of TransIT-LT1 reagent was diluted in 1.5ml of Opti-MEM (Life Technologies) for each 10cm dish, incubated with DNA for 15 min at room temperature (RT) and gently distributed over to the cell medium. After 8 hours, cell medium was changed. 48 hours post-transfection supernatant was collected, filtered through 0.45µm filter and directly stored at -20°C.
Retroviral particles were prepared by transiently transfecting HEK293GP cells with retroviral vectors together with an envelope-producing vector (pMD2-Env) using TransIT-LT1. Transfection and harvest procedure are the same as lentivirus preparation.

Western blot

Cells were washed in HBSS and harvested with lysis buffer (50mM Hepes pH 7.8, 200mM NaCl, 5mM EDTA, 1% NP40, 5% glycerol). In order to obtain protein lysates, extracts were exposed to ultrasound in a sonicator (Diagenode Bioruptor). Cellular extracts were centrifuged for 10 min at 4°C to remove the insoluble fraction and total protein content was determined by Bradford quantification. Samples were boiled at 95°C for 3 min in 1X Sample Buffer (50mM Tris-HCl pH 6.8, 2% SDS, 0.1% Bromophenol Blue, 10% glycerol, 2% 2-mercaptoethanol).
Proteins were run in 4-12% Nupage MOPS acrylamide gels (for LC3 used 12% acrylamide gel) and transferred onto PVDF membranes by wet electrophoretic transfer. Blots were blocked with non-fat dry milk and incubated overnight at 4°C with primary antibodies. Secondary antibodies were incubated for 1 hour at RT, and then blots were developed with chemiluminescent reagents. Images were acquired with Image Quant LAS 4000 (GE healthcare).
The antibodies used in this study were as followed: Anti-YAP/TAZ (63.7; sc-101199) was from Santa Cruz. Anti-GAPDH (MAB347) was from Millipore. Anti-LC3B (NB100-2220) was from Novus.

Immunofluorescence

Cells were plated on fibronectin-coated glass slides and fixed 10 min at room temperature (RT) with 4% PFA solution. Slides were permeabilized for 10 min at RT with PBS 0.3% Triton X-100, and processed for immunofluorescence according to the following conditions: blocking in 10% Goat Serum (GS) in PBST for 1 hour followed by incubation with primary antibody diluted in 2% GS in PBST overnight at 4°C, four washes in PBST and incubation with secondary antibodies diluted in 2% GS in PBST for 1.5 hours at RT. For LAMP1 staining, permeabilization was performed in 80% methanol + 20% acetone, blocking in 5% BSA and diluting primary and secondary antibodies in 2% BSA. After three washes in PBS, samples were counterstained with ProLong-DAPI (Molecular Probes, Life Technologies) to label cell nuclei. Confocal images were obtained with a Leica TCS SP5 equipped with a CCD camera.
Primary antibodies used in this study were: anti-LAMP1 (H4A3, DSHB); Anti-YAP/TAZ (63.7; sc-101199, Santa Cruz); Anti-FLAG (clone M2, A8592, Sigma). Secondary antibodies (Invitrogen) was goat anti-mouse Alexa568.

YAP/TAZ-bound cis-regulatory elements and the genes that they regulate

The list of YAP/TAZ-direct target genes in MDA-MB-231 cells was obtained as previously described (Zanconato et al., 2015). Briefly, a database of YAP/TAZ-binding regions in MDA-MB-231 cells was generated by chromatin immunoprecipitation assays with YAP and TAZ antibodies followed by next-generation sequencing (YAP/TAZ ChIP-Seq). YAP/TAZ peaks were annotated as falling on promoters if they were close to a transcription start site (TSS) (±2 kb); otherwise they were annotated as located in enhancers. YAP/TAZ peaks falling on promoters were assigned to the closest TSS. YAP/TAZ peaks falling on enhancers were annotated using previously reported chromatin interactions loops derived from high-resolution chromatin conformation capture (Hi-C) experiments. This database, describing the YAP/TAZ chromatin "interactome map", was compared with a list of genes regulated by YAP/TAZ obtained by Affymetrix microarrays gene expression analysis, to finally generate a list of direct YAP/TAZ-regulated genes and the corresponding cis-regulatory elements that they bound.

Quantitative real-time PCR (qRT-PCR)

For total RNA extraction, we used the RNeasy Mini Kit (QIAGEN), and contaminant DNA was removed by RNase-Free DNase Set (QIAGEN). cDNA synthesis was carried out with dT-primed MuMLV Reverse Trascriptase (Invitrogen). qRT-PCR analyses were carried out with triplicate samplings on a Rotor-Gene Q (QIAGEN) thermal cycler and analyzed with Rotor-Gene Analysis6.1 software. Expression levels are calculated relative to RPLP0. qRT-PCR oligo sequences are listed in Table 2.

Growth assays

For clonogenic assay, single cells were plated at clonogenic density (300 cells per 10 cm^2 dishes) in complete growth medium. After one week, colonies were fixed and stained with crystal violet solutions.
For soft-agar assay, 15000 cells were suspended in complete growth medium with 0.3% agar and layered on top of 0.6% agar beds. After two weeks, colonies were fixed with 4% PFA.
For mammosphere assay, single cells were plated at 500 cells/cm^2 on ultra-low attachment plates (Costar) in mammosphere medium. Mammospheres were counted after 5 days. The details of mammosphere cultures of MII were described in Zanconato et al., 2015.

ChIP-qPCR

Chromatin immunoprecipitation was performed as described in Zanconato et al., 2015. Briefly, cells were crosslinked with 1% formaldehyde in culture medium for 10 min at RT, and chromatin from lysed nuclei was sheared to 200-600 bp fragments using a Branson Sonifier 450A. For ChIP-qPCR, around 100µg of chromatin was incubated with 3-5µg of antibody overnight at 4°C. Antibody/antigen complexes were recovered with ProteinA-Dynabeads (Invitrogen) for 2 hours at 4°C. qRT-PCR was carried out as described before.
Anti-YAP1(ab52771) was from Abcam; anti-rabbit-IgG (I5006) was from Sigma. qRT-PCR oligo sequences are listed in Table 3.

Mice

C57BL/6J mice were purchased from Charles River. Transgenic lines used in the experiment depicted in Fig. 9 were gently provided by Fernando Camargo (*tetO-YAP^{S127A}*) (Camargo et al., 2007). *R26-rtTAM2* mice (stock #006965) were purchased from The Jackson Laboratory. Animals were genotyped with the recommended set of primers. Animal experiments were performed adhering to our institutional guidelines as approved by OPBA.
To obtain *R26-rtTAM2/+; tetO-YAP^{S127A}* mice, we crossed *R26-rtTAM2/+* mice with *tetO-YAPS^{127A}* mice.

Pancreatic acinar cell isolation and induction of yDucts

Primary pancreatic acini were isolated from the pancreata of 6- to 9-week-old mice according to procedures described in Panciera, et al., 2016. In short, digested tissue was filtered through a 100µm nylon cell strainer. The quality of the isolated acinar tissue was checked under the microscope. For culture of entire acini, explants were seeded in neutralized rat tail collagen type I/acinar culture medium (1:1), overlaid with the acinar culture medium once collagen formed a gel. The acinar culture medium was described in Panciera, et al., 2016. For induction of pancreatic organoids, entire acini of the indicated genotypes were cultured in medium supplemented with 2µg/ml doxycycline for 7 days and organoid formation was morphologically followed.

Matrigel culture of yDucts organoids

To show the self-renewal capacity of pancreatic organoids, yDuct organoids were recovered from collagen cultures, trypsinized to obtain a single cell suspension and re-seeded in 100% Matrigel. Once Matrigel formed a gel, cells were supplemented with pancreatic organoid medium (as described in Panciera, et al., 2016). For analysis, organoids were recovered from Matrigel and processed for protein extraction.

Primary mammary epithelial cell isolation and induction of yMaSCs

Primary mammary epithelial cells were isolated from the mammary glands of 8- to 12-week-old virgin C57BL/6J mice and were sorted into LD cells, LP cells, and MaSCs following the procedures described in Panciera, et al., 2016.
For induction of yMaSCs, LD cells were transduced for 48 hours with FUW-tetO-YAP in combination with rtTA-encoding lentiviruses. After infection, adherent cells were treated with 2μg/ml doxycycline for 7 days in MG colony medium for activating tetracycline-inducible gene expression to obtain yMaSCs. Then cells were detached with trypsin and seeded in 24-well ultralow attachment plates in MG colony medium as described in Panciera, et al., 2016.

Matrigel culture of mammary colonies and organoids

To show the self-renewal capacity of yMaSCs, primary colonies were recovered from the colony medium by collecting the samples and incubation with an excess volume of ice cold HBSS in order to solubilize Matrigel. After 1 hour, colonies were rinsed 3 times in cold HBSS by centrifugation at 1000 rpm for 5 min and then trypsinized to obtain single-cell suspension. Cells were counted and re-seeded in MG colony medium in 24-well ultralow attachment plates for further passaging.
For mammary organoid formation, primary colonies were recovered from the colony medium by collecting the samples and incubation with an excess volume of ice cold HBSS in order to solubilize Matrigel. After 1 hour, colonies were rinsed 3 times in cold HBSS by centrifugation at 1000 rpm for 5 min and then trypsinized to obtain single-cell suspension. Cells were counted and re-seed in 100% Matrigel at 1000 cells/well in 24-well ultralow attachment plates. After Matrigel formed a gel at 37°C, MG organoid medium as described in Panciera, et al., 2016 was added on top.

GFP-LC3 quantification

The quantification of GFP-LC3 puncta area was performed using ImageJ (NIH Image). Each RGB image was splitted into single-color channel and the green channel was converted to grayscale. The region of interest or the cell to be analyzed

was selected using the polygon selection tool (ROI) and a threshold was manually set for minimal and maximal pixel values to trace the GFP-LC3 puncta. Once pixels were thresholded, the area per cell occupied by the GFP-LC3 puncta was measured and shown in arbitrary units (A.U.). The threshold settings remained constant for the analysis of all the images throughout each experiment. If more than one cell were included in the ROI (i.e. for the quantification of "Dense" culture conditions), the area occupied by the GFP-LC3 puncta was normalized to the number of nuclei in the ROI.

For the quantification in Fig. 3B,D an alternative quantification method was applied. Cells with more than ten GFP-LC3 puncta were scored as positive and results were shown as percentage of cells with more than ten GFP-LC3 puncta.

Statistics

The number of biological and technical replicates is indicated in figure legends and text. All statistics were conducted using GraphPad Prism 7.0. Differences at $P<0.05$ were considered statistically significant.

REFERENCES

Aragona, M., Panciera, T., Manfrin, A., Giulitti, S., Michielin, F., Elvassore, N., … Piccolo, S. (2013). A mechanical checkpoint controls multicellular growth through YAP/TAZ regulation by actin-processing factors. *Cell*. https://doi.org/10.1016/j.cell.2013.07.042

Azzolin, L., Panciera, T., Soligo, S., Enzo, E., Bicciato, S., Dupont, S., … Piccolo, S. (2014). YAP/TAZ incorporation in the β-catenin destruction complex orchestrates the Wnt response. *Cell*. https://doi.org/10.1016/j.cell.2014.06.013

Baek, S. H., & Kim, K. Il. (2017). Epigenetic Control of Autophagy: Nuclear Events Gain More Attention. *Molecular Cell*. https://doi.org/10.1016/j.molcel.2016.12.027

Bhat, K. P. L., Salazar, K. L., Balasubramaniyan, V., Wani, K., Heathcock, L., Hollingsworth, F., … Aldape, K. D. (2011). The transcriptional coactivator TAZ regulates mesenchymal differentiation in malignant glioma. *Genes and Development*. https://doi.org/10.1101/gad.176800.111

Camargo, F. D., Gokhale, S., Johnnidis, J. B., Fu, D., Bell, G. W., Jaenisch, R., & Brummelkamp, T. R. (2007). YAP1 Increases Organ Size and Expands Undifferentiated Progenitor Cells. *Current Biology*. https://doi.org/10.1016/j.cub.2007.10.039

Cao, X., Pfaff, S. L., & Gage, F. H. (2008). YAP regulates neural progenitor cell number via the TEA domain transcription factor. *Genes and Development*. https://doi.org/10.1101/gad.1726608

Carroll, B., Mohd-Naim, N., Maximiano, F., Frasa, M. A., McCormack, J., Finelli, M., … Braga, V. M. M. (2013). The TBC/RabGAP Armus Coordinates Rac1 and Rab7 Functions during Autophagy. *Developmental Cell*, *25*(1), 15–28. https://doi.org/10.1016/j.devcel.2013.03.005

Cicchini, M., Karantza, V., & Xia, B. (2015). Molecular Pathways : Autophagy in Cancer — A Matter of Timing and Context, *21*(3), 498–505. https://doi.org/10.1158/1078-0432.CCR-13-2438

Cordenonsi, M., Zanconato, F., Azzolin, L., Forcato, M., Rosato, A., Frasson, C., … Piccolo, S. (2011). The hippo transducer TAZ confers cancer stem cell-related traits on breast cancer cells. *Cell*. https://doi.org/10.1016/j.cell.2011.09.048

Croci, O., De Fazio, S., Biagioni, F., Donato, E., Caganova, M., Curti, L., … Campaner, S. (2017). Transcriptional integration of mitogenic and mechanical signals by Myc and YAP. *Genes and Development*. https://doi.org/10.1101/gad.301184.117

Cufí, S., Vazquez-Martin, A., Oliveras-Ferraros, C., Martin-Castillo, B., Vellon, L., & Menendez, J. A. (2011). Autophagy positively regulates the CD44+CD24-/lowbreast cancer stem-like phenotype. *Cell Cycle*. https://doi.org/10.4161/cc.10.22.17976

Dong, J., Feldmann, G., Huang, J., Wu, S., Zhang, N., Comerford, S. A., … Pan, D. (2007). Elucidation of a Universal Size-Control Mechanism in Drosophila and Mammals. *Cell*. https://doi.org/10.1016/j.cell.2007.07.019

Dupont, S., Morsut, L., Aragona, M., Enzo, E., Giulitti, S., Cordenonsi, M., … Piccolo, S. (2011). Role of YAP/TAZ in mechanotransduction. *Nature*. https://doi.org/10.1038/nature10137

Guo, J. Y., Chen, H. Y., Mathew, R., Fan, J., Strohecker, A. M., Karsli-Uzunbas, G., … White, E. (2011). Activated Ras requires autophagy to maintain oxidative metabolism and tumorigenesis. *Genes and Development*, *25*(5), 460–470. https://doi.org/10.1101/gad.2016311

Halder, G., & Johnson, R. L. (2011). Hippo signaling: growth control and beyond. *Development*. https://doi.org/10.1242/dev.045500

Huang, J., Wu, S., Barrera, J., Matthews, K., & Pan, D. (2005). The Hippo signaling pathway coordinately regulates cell proliferation and apoptosis by inactivating Yorkie, the Drosophila homolog of YAP. *Cell*. https://doi.org/10.1016/j.cell.2005.06.007

Janmey, P. A., & Miller, R. T. (2011). Mechanisms of mechanical signaling in development and disease. *Journal of Cell Science*. https://doi.org/10.1242/jcs.071001

Johnson, R., & Halder, G. (2014). The two faces of Hippo: Targeting the Hippo pathway for regenerative medicine and cancer treatment. *Nature Reviews Drug Discovery*. https://doi.org/10.1038/nrd4161

Kang, M. R., Kim, M. S., Oh, J. E., Kim, Y. R., Song, S. Y., Kim, S. S., … Lee, S. H. (2009). Frameshift mutations of autophagy-related genes ATG2B, ATG5, ATG9B and ATGI2 in gastric and colorectal cancers with microsatellite instability. *Journal of Pathology*. https://doi.org/10.1002/path.2509

Kern, A., Dikic, I., & Behl, C. (2015). The integration of autophagy and cellular trafficking pathways via RAB GAPs. *Autophagy*. https://doi.org/10.1080/15548627.2015.1110668

Khaminets, A., Behl, C., & Dikic, I. (2016). Ubiquitin-Dependent And Independent Signals In Selective Autophagy. *Trends in Cell Biology*. https://doi.org/10.1016/j.tcb.2015.08.010

King, J. S. (2012). Mechanical stress meets autophagy: Potential implications for physiology and pathology. *Trends in Molecular Medicine*. https://doi.org/10.1016/j.molmed.2012.08.002

Klionsky, D. J., Klionsky, D. J., Abdelmohsen, K., Abe, A., Abedin, M. J., Abeliovich, H., … Zughaier, S. M. (2016). Guidelines for the use and interpretation of assays for monitoring autophagy (3rd edition). *Autophagy*, *12*(1), 1–222. https://doi.org/10.1080/15548627.2015.1100356

Lee, K.-P., Lee, J.-H., Kim, T.-S., Kim, T.-H., Park, H.-D., Byun, J.-S., … Lim, D.-S. (2010). The Hippo-Salvador pathway restrains hepatic oval cell proliferation, liver size, and liver tumorigenesis. *Proceedings of the National Academy of Sciences*. https://doi.org/10.1073/pnas.0912203107

Liang, X. H., Jackson, S., Seaman, M., Brown, K., Kempkes, B., Hibshoosh, H., & Levine, B. (1999). Induction of autophagy and inhibition of tumorigenesis by beclin 1. *Nature*. https://doi.org/10.1038/45257

Ma, T., Li, J., Xu, Y., Yu, C., Xu, T., Wang, H., … Ding, S. (2015). Atg5-independent autophagy regulates mitochondrial clearance and is essential for iPSC reprogramming. *Nature Cell Biology*. https://doi.org/10.1038/ncb3256

Martin, K., Pritchett, J., Llewellyn, J., Mullan, A. F., Athwal, V. S., Dobie, R., … Hanley, K. P. (2016). PAK proteins and YAP-1 signalling downstream of integrin beta-1 in myofibroblasts promote liver fibrosis. *Nature Communications*. https://doi.org/10.1038/ncomms12502

Mizushima, N. (2007). Autophagy: Process and function. *Genes and Development*. https://doi.org/10.1101/gad.1599207

Mizushima, N. (2009). Chapter 2 Methods for Monitoring Autophagy Using GFP-LC3 Transgenic Mice. *Methods in Enzymology*. https://doi.org/10.1016/S0076-6879(08)03602-1

Mizushima, N., & Yoshimori, T. (2007). How to interpret LC3 immunoblotting. *Autophagy*. https://doi.org/10.4161/auto.4600

Mizushima, N., Yoshimori, T., & Levine, B. (2010). Methods in Mammalian Autophagy Research. *Cell*, *140*(3), 313–326. https://doi.org/10.1016/j.cell.2010.01.028

Mo, J.-S., Park, H. W., & Guan, K.-L. (2014). The Hippo signaling pathway in stem

cell biology and cancer. *EMBO Reports*, *15*(6), 642–656. https://doi.org/10.15252/embr.201438638

Nuschke, A., Rodrigues, M., Stolz, D. B., Chu, C. T., Griffith, L., & Wells, A. (2014). Human mesenchymal stem cells/multipotent stromal cells consume accumulated autophagosomes early in differentiation. *Stem Cell Research and Therapy*. https://doi.org/10.1186/scrt530

Panciera, T., Azzolin, L., Fujimura, A., Di Biagio, D., Frasson, C., Bresolin, S., … Piccolo, S. (2016). Induction of Expandable Tissue-Specific Stem/Progenitor Cells through Transient Expression of YAP/TAZ. *Cell Stem Cell*, *19*(6), 725–737. https://doi.org/10.1016/j.stem.2016.08.009

Panciera, T., Azzolin, L., Fujimura, A., Rosato, A., Cordenonsi, M., & Correspondence, S. P. (2016). Induction of Expandable Tissue-Specific Stem/ Progenitor Cells through Transient Expression of YAP/TAZ. *Stem Cell*. https://doi.org/10.1016/j.stem.2016.08.009

Piccolo, S., Dupont, S., & Cordenonsi, M. (2014). The Biology of YAP/TAZ: Hippo Signaling and Beyond. *Physiological Reviews*, *94*(4), 1287–1312. https://doi.org/10.1152/physrev.00005.2014

Puri, P., & Chandra, A. (2014). Autophagy modulation as a potential therapeutic target for liver diseases. *Journal of Clinical and Experimental Hepatology*. https://doi.org/10.1016/j.jceh.2014.04.001

Sakamaki, J. ichi, Wilkinson, S., Hahn, M., Tasdemir, N., O'Prey, J., Clark, W., … Ryan, K. M. (2017). Bromodomain Protein BRD4 Is a Transcriptional Repressor of Autophagy and Lysosomal Function. *Molecular Cell*. https://doi.org/10.1016/j.molcel.2017.04.027

Salemi, S., Yousefi, S., Constantinescu, M. A., Fey, M. F., & Simon, H.-U. (2012). Autophagy is required for self-renewal and differentiation of adult human stem cells. *Cell Research*. https://doi.org/10.1038/cr.2011.200

Santner, S. J., Dawson, P. J., Tait, L., Soule, H. D., Eliason, J., Mohamed, A. N., … Miller, F. R. (2001). Malignant MCF10CA1 cell lines derived from premalignant human breast epithelial MCF10AT cells. *Breast Cancer Research and Treatment*. https://doi.org/10.1023/A:1006461422273

Takamura, A., Komatsu, M., Hara, T., Sakamoto, A., Kishi, C., Waguri, S., … Hino, O. (2011). Autophagy-deficient mice develop multiple liver tumors, *5*, 795–800. https://doi.org/10.1101/gad.2016211.many

Tanida, I., Minematsu-Ikeguchi, N., Ueno, T., & Kominami, E. (2005). Lysosomal turnover, but not a cellular level, of endogenous LC3 is a marker for autophagy. *Autophagy*, *1*(2), 84–91. https://doi.org/10.4161/auto.1.2.1697

Totaro, A., Castellan, M., Battilana, G., Zanconato, F., Azzolin, L., Giulitti, S., … Piccolo, S. (2017). YAP/TAZ link cell mechanics to Notch signalling to control epidermal stem cell fate. *Nature Communications*. https://doi.org/10.1038/ncomms15206

Totaro, A., Panciera, T., & Piccolo, S. (2018). YAP/TAZ upstream signals and downstream responses. *Nature Cell Biology*. https://doi.org/10.1038/s41556-018-0142-z

Toyofuku, T., Morimoto, K., Sasawatari, S., & Kumanogoh, A. (2015). Leucine-Rich Repeat Kinase 1 Regulates Autophagy through Turning On TBC1D2-Dependent Rab7 Inactivation. *Molecular and Cellular Biology*, *35*(17), 3044–3058. https://doi.org/10.1128/MCB.00085-15

Tra, T., Gong, L., Kao, L. P., Li, X. L., Grandela, C., Devenish, R. J., … Prescott, M. (2011). Autophagy in human embryonic stem cells. *PLoS ONE*. https://doi.org/10.1038/labinvest.2015.84

von Gise, A., Lin, Z., Schlegelmilch, K., Honor, L. B., Pan, G. M., Buck, J. N., … Pu, W. T. (2012). YAP1, the nuclear target of Hippo signaling, stimulates heart

growth through cardiomyocyte proliferation but not hypertrophy. *Proceedings of the National Academy of Sciences*. https://doi.org/10.1073/pnas.1116136109

Wang, S., Xia, P., Ye, B., Huang, G., Liu, J., & Fan, Z. (2013). Transient Activation of Autophagy via Sox2-Mediated Suppression of mTOR Is an Important Early Step in Reprogramming to Pluripotency. *Cell Stem Cell*. https://doi.org/10.1016/j.stem.2013.10.005

Wei, H., Wei, S., Gan, B., Peng, X., Zou, W., & Guan, J. L. (2011). Suppression of autophagy by FIP200 deletion inhibits mammary tumorigenesis. *Genes and Development*. https://doi.org/10.1101/gad.2051011

White, E. (2012). Deconvoluting the context-dependent role for autophagy in cancer. *Nature Reviews.Cancer*, *12*(6), 401–410. https://doi.org/10.1038/nrc3262 [doi]

Yang, S., Wang, X., Contino, G., Liesa, M., Sahin, E., Ying, H., … Kimmelman, A. C. (2011). Pancreatic cancers require autophagy for tumor growth. *Genes and Development*. https://doi.org/10.1101/gad.2016111

Yu, F. X., & Guan, K. L. (2013). The Hippo pathway: Regulators and regulations. *Genes and Development*. https://doi.org/10.1101/gad.210773.112

Yue, Z., Jin, S., Yang, C., Levine, A. J., & Heintz, N. (2003). Beclin 1 , an autophagy gene essential for early embryonic development , is a haploinsufficient tumor suppressor, *100*(25).

Zanconato, F., Battilana, G., Forcato, M., Filippi, L., Azzolin, L., Manfrin, A., … Bicciato, S. (2018). mediated by YAP / TAZ through BRD4. *Nature Medicine*, *24*(October). https://doi.org/10.1038/s41591-018-0158-8

Zanconato, F., Cordenonsi, M., & Piccolo, S. (2016). YAP/TAZ at the Roots of Cancer. *Cancer Cell*, *29*(6), 783–803.

https://doi.org/10.1016/j.ccell.2016.05.005

Zanconato, F., Forcato, M., Battilana, G., Azzolin, L., Quaranta, E., Bodega, B., … Piccolo, S. (2015). Genome-wide association between YAP/TAZ/TEAD and AP-1 at enhancers drives oncogenic growth. *Nature Cell Biology*, *17*(9), 1218–1227. https://doi.org/10.1038/ncb3216

Zhao, B., Li, L., Lei, Q., & Guan, K. L. (2010). The Hippo-YAP pathway in organ size control and tumorigenesis: An updated version. *Genes and Development*. https://doi.org/10.1101/gad.1909210

Zhao, B., Ye, X., Yu, J., Li, L., Li, W., Li, S., … Guan, K. L. (2008). TEAD mediates YAP-dependent gene induction and growth control. *Genes and Development*. https://doi.org/10.1101/gad.1664408

Zhou, D., Conrad, C., Xia, F., Park, J. S., Payer, B., Yin, Y., … Bardeesy, N. (2009). Mst1 and Mst2 Maintain Hepatocyte Quiescence and Suppress Hepatocellular Carcinoma Development through Inactivation of the Yap1 Oncogene. *Cancer Cell*. https://doi.org/10.1016/j.ccr.2009.09.026

TABLES

Table 1: list of siRNAs sequences

siRNA	Sense-strand sequence
siYAP1	GACAUCUUCUGGUCAGAGA dTdT
siYAP2	CUGGUCAGAGAUACUUCUU dTdT
siYAP3	GGUGAUACUAUCAACCAAA dTdT
siTAZ1	ACGUUGACUUAGGAACUUU dTdT
siTAZ2	AGAGGUACUUCCUCAAUCA dTdT
siTAZ3	AGGUACUUCCUCAAUCACA dTdT
siTBC1D2 A	CGGACAGUCUCAUUAGCAA dTdT
siTBC1D2 B	GCAAGUACCUGGCCGGUCU dTdT
siTBC1D2 C	GCAACACGCUGACGGCAUC dTdT
siATG7	CGAGUAUCGGCUGGAUGAA dTdT

Table 2: List of primers for qRT-PCR

Gene	Primer	Sequence
RPLP0	Forward	CGGATTACACCTTCCCACTTG
	Reverse	CCGACTCTTCCTTGGCTTCA
CTGF	Forward	AGGAGTGGGTGTGTGACGA
	Reverse	CCAGGCAGTTGGCTCTAATC
TBC1D2	Forward	TTGCCCTGCTGGTCCTAGAG
	Reverse	GGTGACGAGGGAGAGATCCA

Table 3: List of primers for Chip-qPCR

Gene	Primer	Sequence
CYR61	Forward	CACACACAAAGGTGCAATGGAG
	Reverse	CCGGAGCCCGCCTTTTATAC
TBC1D2	Forward	AAGTCAGCTTCTCAGGGCTCA
	Reverse	TTGAGGGAAAGACACCCACTG

FIGURES

Figure 1 YAP/TAZ control autophagy flux in mammary epithelial cells by regulating the fusion of autophagosomes with lysosomes.

(A-B) Immunoblot analysis for YAP/TAZ and LC3 in MDA-MB-231 (A) and MCF10A (B) transfected with control siRNA (siCo.) or two independent YAP/TAZ siRNA mixes (siYAP/TAZ #1 or siYAP/TAZ #2) for 48 hours. The cleaved LC3 peptide and its phosphatidylethanolamine conjugated form are indicated as LC3-I and LC3-II respectively. GAPDH serves as loading control.

(C) Representative confocal images of MDA-MB-231-GFP-LC3 cells transfected with control siRNA (siCo.) or two independent YAP/TAZ siRNA mixes (siYAP/TAZ #1 or siYAP/TAZ #2) for 48 hours. Cells were treated without (-CQ) or with 50μM CQ (+CQ) for the last 4 hours. GFP-LC3 (green); DAPI (blue) is a nuclear counterstain. Scale bar: 20μm.

(D) Quantification of GFP-LC3 puncta accumulation induced by YAP/TAZ knockdown as in (C), measured as area of GFP-LC3 puncta per cell and shown in arbitrary units (A.U.). At least 50 cells were scored for each condition from three independent experiments. Bars represent mean + SEM (*P<0.01 compared to -CQ siCo; Student's *t*-test). See Methods and Materials section for GFP-LC3 puncta area quantification method.

(E) Representative confocal images of MII-MB-231-GFP-LC3 cells transfected with control siRNA (siCo.) or two independent YAP/TAZ siRNA mixes (siYAP/TAZ #1 or siYAP/TAZ #2) for 48 hours. Cells were treated without (-CQ) or with 50μM CQ (+CQ) for the last 4 hours. GFP-LC3 (green); DAPI (blue) is a nuclear counterstain. Scale bar: 20μm.

(F) Quantification of GFP-LC3 puncta accumulation induced by YAP/TAZ knockdown as in (E), measured as area of GFP-LC3 puncta per cell and shown in arbitrary units (A.U.). At least 50 cells were scored for each condition from three independent experiments. Bars represent mean + SEM (*P<0.01 compared to -CQ siCo; Student's *t*-test).

(G) Representative confocal images of GFP-LC3 (green) and LAMP1 (red) in MDA-MB-231-GFP-LC3 transfected with control siRNA (siCo.) or two independent YAP/TAZ siRNAs mixes (siYAP/TAZ #1 and siYAP/TAZ #2) for 48 hours. DAPI (blue) is a nuclear counterstain. Scale bar: 20μm.

(H) Quantification of the colocalization between LAMP1-positive vesicles (red) and GFP-LC3 puncta (green) as in (G), scored as the ratio of the double-positive vesicles (yellow) on the total of GFP-LC3 puncta (green) per cell. At least 20 cells were scored for each condition from three independent experiments. Data are presented as box and whisker plots; whiskers extend to show the highest and lowest values (*P<0.0001 compared to siCo; one-way analysis of variance (ANOVA)).

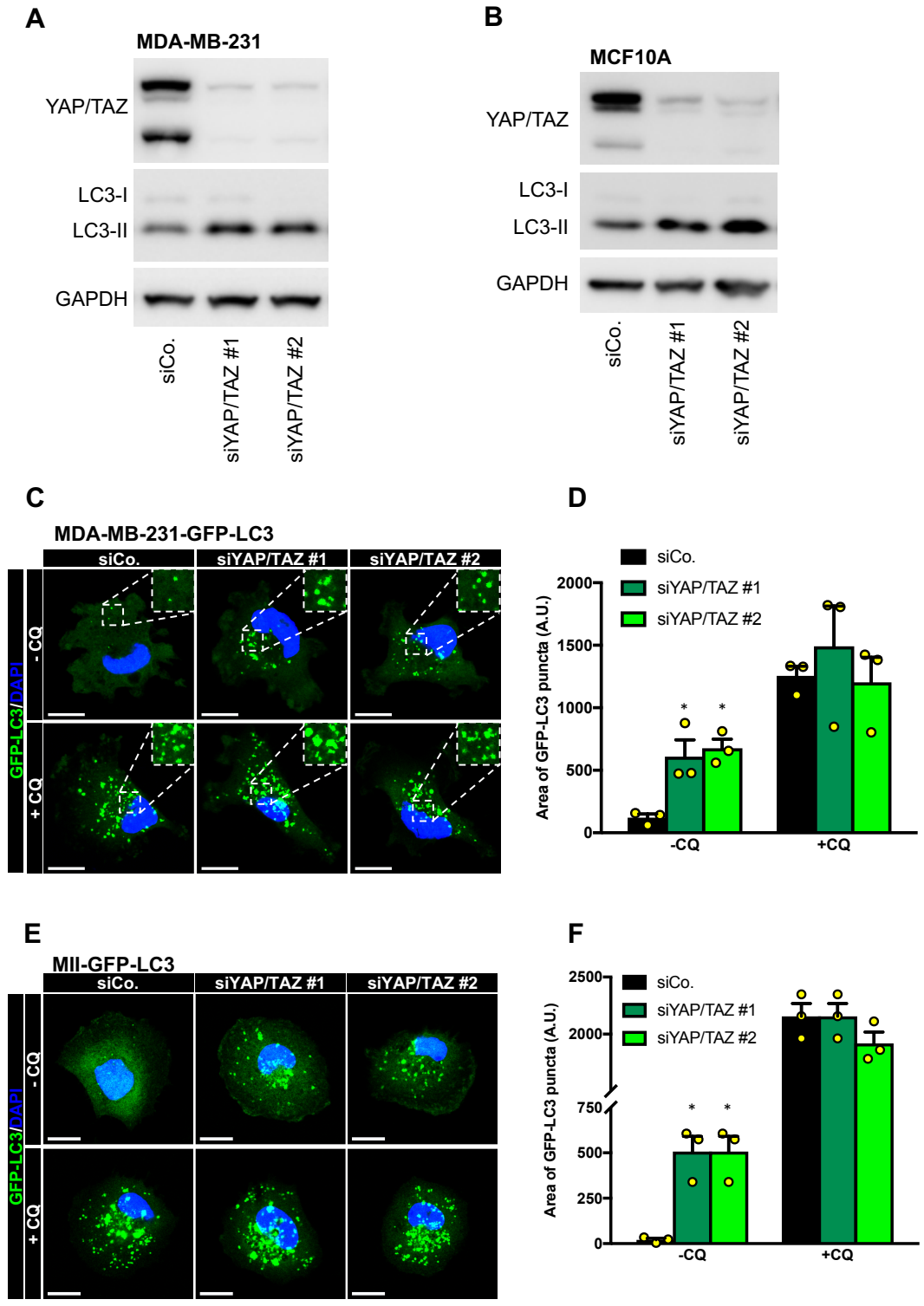
A
MDA-MB-231
YAP/TAZ
LC3-I
LC3-II
GAPDH
siCo.
siYAP/TAZ #1
siYAP/TAZ #2
B
MCF10A
YAP/TAZ
LC3-I
LC3-II
GAPDH
siCo.
siYAP/TAZ #1
siYAP/TAZ #2
C
MDA-MB-231-GFP-LC3
siCo.
siYAP/TAZ #1
siYAP/TAZ #2
GFP-LC3/DAPI
- CQ
+ CQ
D
siCo.
siYAP/TAZ #1
siYAP/TAZ #2
Area of GFP-LC3 puncta (A.U.)
2000
1500
1000
500
0
-CQ
+CQ
E
MII-GFP-LC3
siCo.
siYAP/TAZ #1
siYAP/TAZ #2
GFP-LC3/DAPI
- CQ
+ CQ
F
siCo.
siYAP/TAZ #1
siYAP/TAZ #2
Area of GFP-LC3 puncta (A.U.)
2500
2000
750
500
250
0
-CQ
+CQ

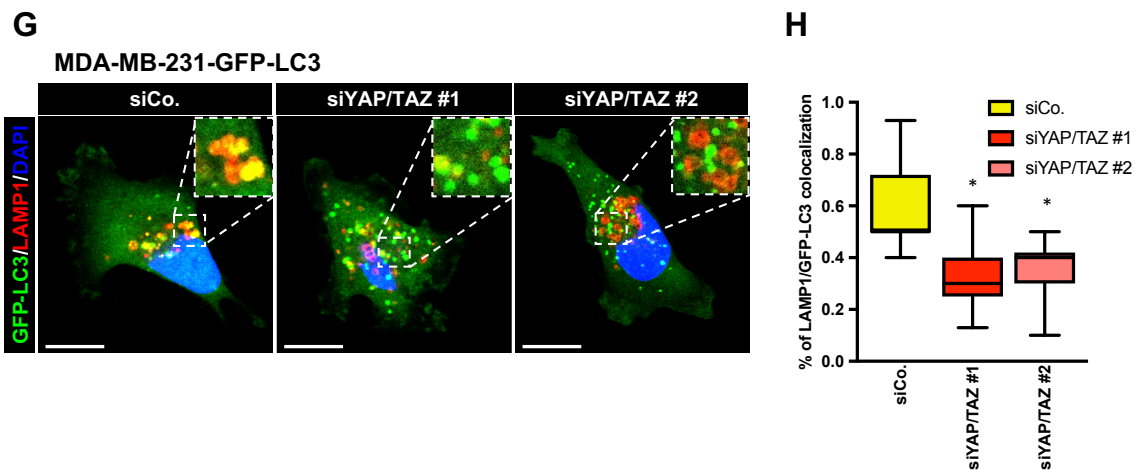
G
MDA-MB-231-GFP-LC3
siCo.
siYAP/TAZ #1
siYAP/TAZ #2
GFP-LC3/LAMP1/DAPI
H
% of LAMP1/GFP-LC3 colocalization
1.0
0.8
0.6
0.4
0.2
0.0
siCo.
siYAP/TAZ #1
siYAP/TAZ #2
*
*
siCo.
siYAP/TAZ #1
siYAP/TAZ #2

Figure 1

Figure 2 YAP/TAZ control of the autophagic flux depends on their transcriptional activity.

(A-C) MII-GFP-LC3 were infected with an empty lentiviral vector (Empty) or with the indicated siRNA-insensitive doxycycline-inducible lentiviral YAP constructs fused to an N-terminal FLAG tag. Cells were transfected with either control (siCo.) or YAP/TAZ siRNAs (siYAP/TAZ), treated with 2µg/ml doxycycline and analyzed 48 hours after siRNA transfection. (A-B) For fluorescence analysis cells were also treated with or without CQ for the last 4 hours before fixation.

(A) Representative confocal images of GFP-LC3 (green) and FLAG-tag staining (red) in MII-GFP-LC3 as described above. DAPI (blue) is a nuclear counterstain. Scale bar: 20µm.

(B) Quantification of GFP-LC3 puncta of MII-GFP-LC3 cells treated as in (A), measured as area of GFP-LC3 puncta per cell and shown in arbitrary units (A.U.). At least 50 Empty-infected cells or FLAG-tag positive cells were scored for each condition from three independent experiments. Bars represent mean + SEM ($^{\S}P<0.05$ compared to -CQ Empty-infected siCo; $^{*}P<0.05$ compared to -CQ Empty-infected siYAP/TAZ; one-way ANOVA).

(C) qRT-PCR analysis of CTGF mRNA levels normalized to RPLP0 from MII-GFP-LC3 treated as in (A). Values were normalized to the Empty-infected cells transfected with siCo (siCo, green bar). Bars represent mean + S.D. ($^{*}P<0.001$ compared to Empty-infected siCo; $^{\S}P<0.0001$ compared to Empty-infected siYAP/TAZ; one-way ANOVA).

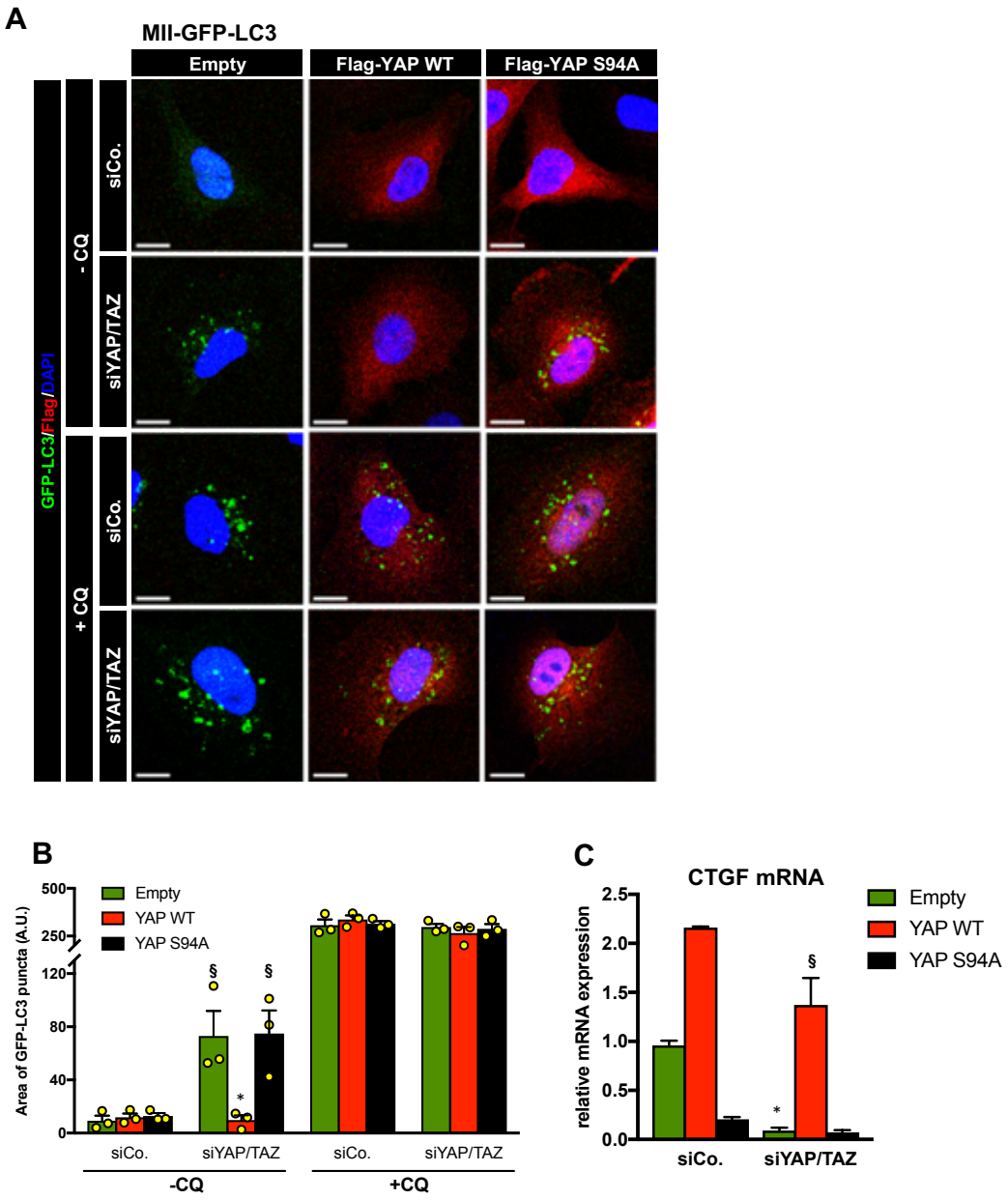
A
MII-GFP-LC3
Empty
Flag-YAP WT
Flag-YAP S94A
GFP-LC3/Flag/DAPI
- CQ
+ CQ
siCo.
siYAP/TAZ
B
Area of GFP-LC3 puncta (A.U.)
500
250
120
80
40
0
Empty
YAP WT
YAP S94A
§
*
siCo.
siYAP/TAZ
-CQ
+CQ
C
CTGF mRNA
relative mRNA expression
2.5
2.0
1.5
1.0
0.5
0.0
Empty
YAP WT
YAP S94A
§
*
siCo.
siYAP/TAZ

Figure 2

Figure 3 ECM elasticity or cell density regulate autophagy through YAP/TAZ

(A) Representative confocal images of GFP-LC3 (green) and YAP/TAZ (red) in MII-GFP-LC3 cells plated on fibronectin-coated coverslips (Stiff) or acrylamide hydrogels of 2kPa (Soft) for 24 hours. Cells were treated without (-CQ) or with 50μM CQ (+CQ) for the last 4 hours. DAPI (blue) is a nuclear counterstain. Scale bar: 20μm.

(B) Percentage of MII-GFP-LC3 cells accumulating GFP-LC3 puncta according to (A). Cells with more than ten GFP-LC3 puncta were scored as positive. More than 50 cells were scored for each condition from three independent experiments. Bars represent mean + SEM (*P<0.0001 compared to -CQ stiff; one-way ANOVA). See Methods and Materials section for the quantification method of GFP-LC3 puncta positive cell.

(C) Proportion of MII-GFP-LC3 displaying preferential nuclear YAP/TAZ localization (N, red), even distribution of YAP/TAZ in nucleus and cytoplasm (E, pink) or cytoplasmic YAP/TAZ (C, white) according to (A). More than 50 cells were scored for each condition from three independent experiments. Bars represent mean + SEM.

(D) MII-GFP-LC3 cells were infected with either an empty lentiviral vector (Empty) or with the indicated doxycycline-inducible lentiviral YAP constructs. Cells were plated on fibronectin-coated acrylamide hydrogels of 2kPa and treated with 2μg/ml doxycycline for 24 hours. Cells were treated without (-CQ) or with 50μM CQ (+CQ) for the last 4 hours and finally analyzed. Graph shows the percentage of MII-GFP-LC3 accumulating GFP-LC3 puncta. At least 50 cells were scored for each condition from three independent experiments. Bars represent mean + SEM (*P<0.001 compared to -CQ Empty-infected; one-way ANOVA).

(E) Representative confocal images of MII-GFP-LC3 cells infected with either an empty lentiviral vector (Empty) or with a doxycycline-inducible lentiviral YAP constructs (YAP), plated for 24 hours in the presence of doxycycline as low-density (Sparse) or high-density (Dense) cultures. Cells were treated without (-CQ) or with 50μM CQ (+CQ) for the last 4 hours. GFP-LC3 (green); DAPI (blue) is a nuclear counterstain. Scale bar: 20μm. See Methods and Materials section for the experimental setting of Sparse and Dense cultures.

(F) Quantification of GFP-LC3 puncta of MII-GFP-LC3 cells treated as in (E), measured as area of GFP-LC3 puncta per cell and shown in arbitrary units (A.U.). At least 100 cells were scored for each condition from three independent experiments. Bars represent mean + SEM (*P<0.001 compared to -CQ Sparse; one-way ANOVA).

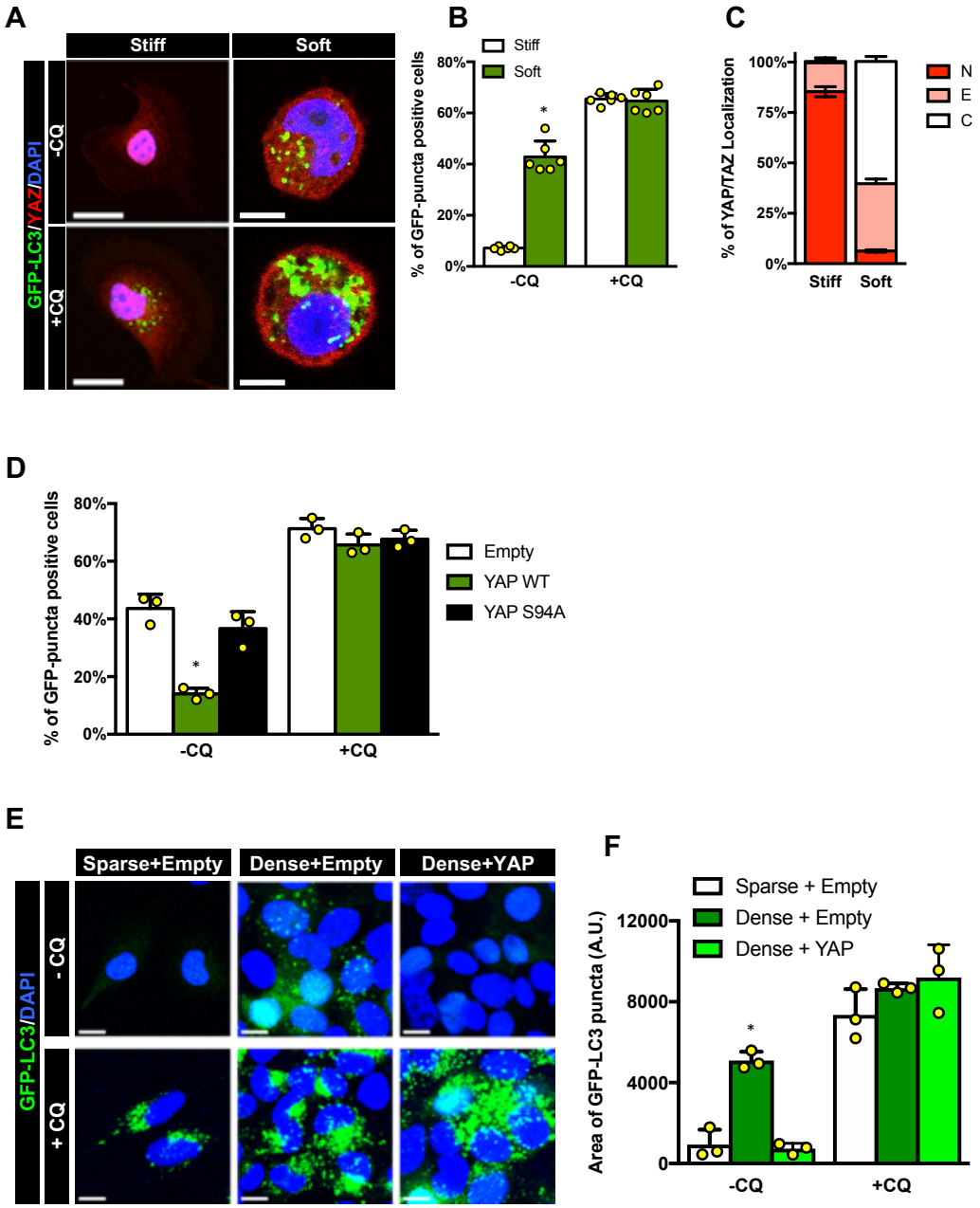
A
Stiff
Soft
GFP-LC3/YAZ/DAPI
-CQ
+CQ
B
Stiff
Soft
% of GFP-puncta positive cells
80%
60%
40%
20%
0%
*
-CQ
+CQ
C
% of YAP/TAZ Localization
100%
75%
50%
25%
0%
N
E
C
Stiff
Soft
D
% of GFP-puncta positive cells
80%
60%
40%
20%
0%
*
-CQ
+CQ
Empty
YAP WT
YAP S94A
E
Sparse+Empty
Dense+Empty
Dense+YAP
GFP-LC3/DAPI
- CQ
+ CQ
F
Sparse + Empty
Dense + Empty
Dense + YAP
Area of GFP-LC3 puncta (A.U.)
12000
8000
4000
0
*
-CQ
+CQ

Figure 3

Figure 4 Actomyosin cytoskeleton regulate autophagy.

(A) Representative confocal images of MII-GFP-LC3 cells treated for 16 hours with vehicles (Mock) or 0.4μM latrunculin A (LatA). Cells were treated without (-CQ) or with 50μM CQ (+CQ) for the last 4 hours. GFP-LC3 (green); DAPI (blue) is a nuclear counterstain. Scale bar: 20μm.
(B) Quantification of GFP-LC3 puncta of MII-GFP-LC3 cells treated as in (A), measured as area of GFP-LC3 puncta per cell and shown in arbitrary units (A.U.). At least 50 cells were scored for each condition from three independent experiments. Bars represent mean + SEM (*P<0.05 compared to -CQ Mock-treated cells; one-way ANOVA).
(C) Representative confocal images of MII-GFP-LC3 cells treated for 16 hours with vehicles (Mock), 10μM or 25μM ML-7. GFP-LC3 (green); DAPI (blue) is a nuclear counterstain. Scale bar: 20μm.
(D) Quantification of GFP-LC3 puncta of MII-GFP-LC3 cells treated as in (C), measured as area of GFP-LC3 puncta per cell and shown in arbitrary units (A.U.). At least 50 cells were scored for each condition from three independent experiments. Bars represent mean + SEM (*P<0.05, **P<0.0001 compared to Mock-treated cells; one-way ANOVA).

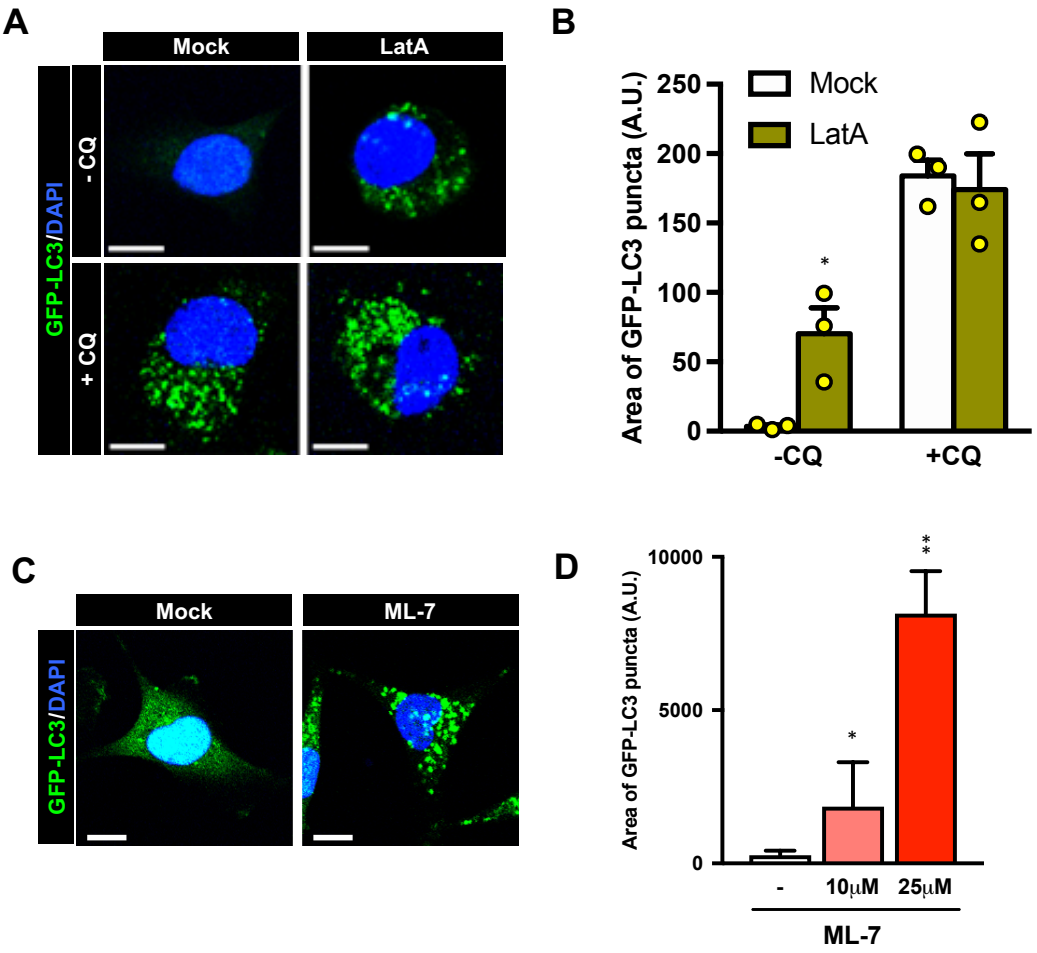
A
Mock
LatA
GFP-LC3/DAPI
- CQ
+ CQ
B
Area of GFP-LC3 puncta (A.U.)
250
200
150
100
50
0
Mock
LatA
*
-CQ
+CQ
C
Mock
ML-7
GFP-LC3/DAPI
D
Area of GFP-LC3 puncta (A.U.)
10000
5000
0
*
**
-
10μM
25μM
ML-7

Figure 4

Figure 5 YAP/TAZ transcriptionally regulate the expression of TBC1D2 gene

(A-B) Validation by ChIP-qPCR in MDA-MB-231 (A) and MII (B) of the YAP/TAZ-binding site on the TBC1D2-associated enhancer identified through combination of YAP/TAZ ChIP-seq and Hi-C. ChIP-qPCR of the CYR61 promoter is a positive control locus; HBB is a negative control locus (Neg Contr.). The TBC1D2 enhancer was enriched in YAP-immunoprecipitated chromatin from control siRNA transfected cells (siCo.), but not in negative control IP (IgG) or in chromatin obtained from YAP/TAZ-depleted cells (siYT). Data from three replicates (mean + S.D.) are shown normalized to the Percent Input (1% of starting chromatin used as Input).

(C-D) Validation of the YAP/TAZ-dependent regulation of TBC1D2 gene. MDA-MB-231 (C) or MII (D) were transfected with either control siRNA (siCo.) or three independent YAP/TAZ siRNA mixes (siYAP/TAZ #1, siYAP/TAZ #2 and siYAP/TAZ #3) for 48 hours. Then cells were harvested for qRT-PCR of TBC1D2 mRNA levels normalized to RPLP0 gene. Data were normalized to the corresponding control siRNA condition (siCo, Black bar). Bars represent mean + S.D. (*P<0.0001 compared to siCo; one-way ANOVA).

(E) MII-GFP-LC3, infected with an empty lentiviral vector (Empty) or with the indicated siRNA-insensitive doxycycline-inducible lentiviral YAP constructs, were transfected either with control (siCo.) or YAP/TAZ-targeting siRNAs (siYAP/TAZ), and treated with 2µg/ml doxycycline. 48 hours after siRNA transfection, cells were harvested and analyzed by qRT-PCR for the mRNA levels of TBC1D2 normalized to RPLP0. Data were normalized to Empty-infected cells transfected with control siRNA (siCo, Black bar). Bars represent mean + S.D. (*P<0.01 compared to Empty-infected siCo; §P<0.001 compared to Empty-infected siYAP/TAZ; one-way ANOVA).

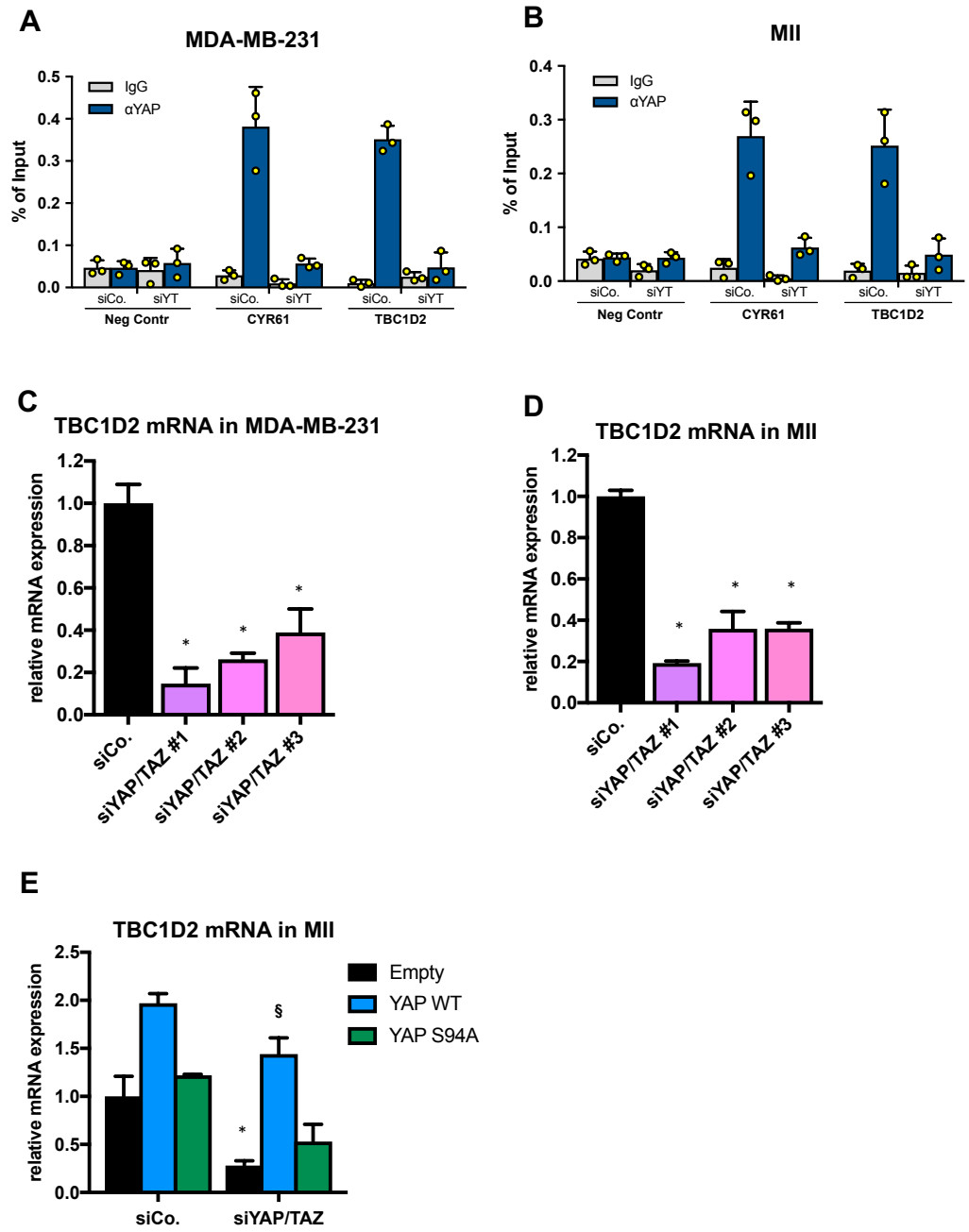
A
MDA-MB-231
IgG
αYAP
% of Input
siCo.
siYT
Neg Contr
CYR61
TBC1D2
B
MII
C
TBC1D2 mRNA in MDA-MB-231
relative mRNA expression
siCo.
siYAP/TAZ #1
siYAP/TAZ #2
siYAP/TAZ #3
D
TBC1D2 mRNA in MII
E
TBC1D2 mRNA in MII
Empty
YAP WT
YAP S94A
siYAP/TAZ

Figure 5

Figure 6 TBC1D2 knockdown is epistatic to YAP/TAZ for autophagy regulation.

(A) qRT-PCR analysis of MDA-MB-231 transfected with either control siRNA (siCo.) or three independent TBC1D2 siRNAs (siTBC1D2 A, siTBC1D2 B and siTBC1D2 C). Graphs show relative levels of TBC1D2 mRNA normalized to RPLP0. Data were normalized to control siRNA condition (siCo, Black bar). Bars represent mean + S.D. (*P<0.0001 compared to siCo; one-way ANOVA).
(B) Immunoblot analysis for LC3 in MDA-MB-231 transfected with control siRNA (siCo.) or two independent TBC1D2 siRNAs (siTBC1D2 A and siTBC1D2 B) for 48 hours. The cleaved LC3 peptide and its phosphatidylethanolamine conjugated form are indicated as LC3-I and LC3-II respectively. GAPDH serves as loading control.
(C) Representative confocal images of MII-GFP-LC3 transfected with either control siRNA (siCo.) or three independent TBC1D2 siRNAs (siTBC1D2 A, siTBC1D2 B and siTBC1D2 C) for 48 hours. Cells were treated without (-CQ) or with 50μM CQ (+CQ) for the last 4 hours. GFP-LC3 (green); DAPI (blue) is a nuclear counterstain. Scale bar: 20μm.
(D) Quantification of GFP-LC3 puncta of MII-GFP-LC3 cells treated as in (C), measured as area of GFP-LC3 puncta per cell and shown in arbitrary units (A.U.). At least 50 cells were scored for each condition from three independent experiments. Bars represent mean + SEM (*P<0.001, **P<0.05 compared to -CQ siCo; one-way ANOVA).
(E) MII-GFP-LC3, infected with an empty lentiviral vector (Empty) or with a siRNA-insensitive doxycycline-inducible lentiviral YAP constructs with N-terminal FLAG tag (FLAG-YAP WT), were transfected with control siRNA (siCo.), YAP/TAZ siRNAs (siYAP/TAZ) or TBC1D2 siRNA (siTBC1D2), and treated with 2μg/ml doxycycline. After 48 hours from siRNA transfection cells were fixed and analyzed for GFP-LC3 puncta. Cells were treated without (-CQ) or with 50μM CQ (+CQ) for the last 4 hours before fixation. Representative confocal images of MII-GFP-LC3 treated as described. GFP-LC3 (green); FLAG-YAP (red); DAPI (blue) is a nuclear counterstain. Scale bar: 20μm.
(F) Quantification of GFP-LC3 puncta of MII-GFP-LC3 cells treated as in (E), measured as area of GFP-LC3 puncta per cell and shown in arbitrary units (A.U.).

At least 50 cells were scored for each condition from three independent experiments. Bars represent mean + SEM (*P<0.05, **P<0.01 compared to lane 1; §P<0.05 compared to lane 4; one-way ANOVA).

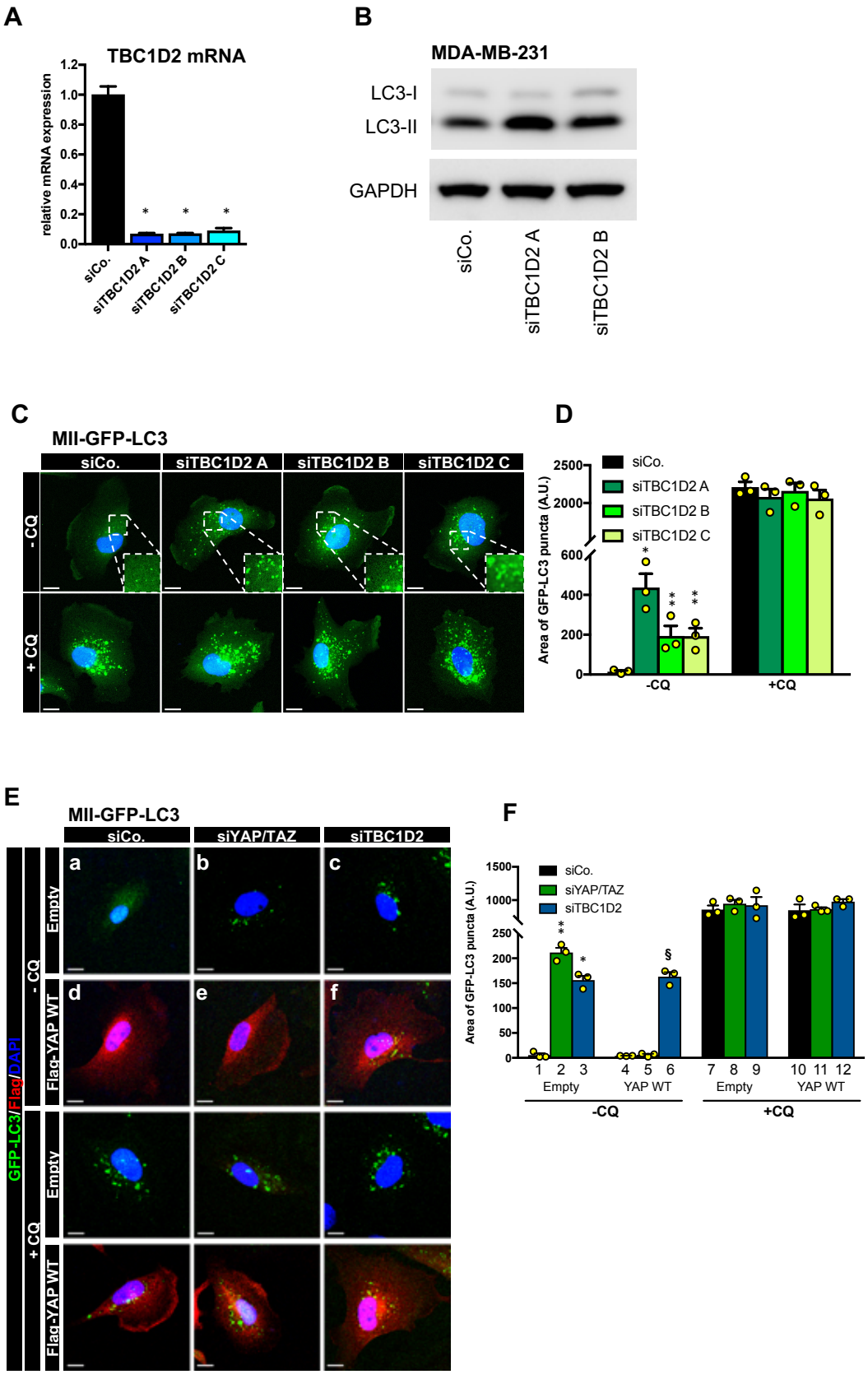
A
TBC1D2 mRNA
relative mRNA expression
1.2
1.0
0.8
0.6
0.4
0.2
0.0
siCo.
siTBC1D2 A
siTBC1D2 B
siTBC1D2 C
B
MDA-MB-231
LC3-I
LC3-II
GAPDH
siCo.
siTBC1D2 A
siTBC1D2 B
C
MII-GFP-LC3
siCo.
siTBC1D2 A
siTBC1D2 B
siTBC1D2 C
- CQ
+ CQ
D
siCo.
siTBC1D2 A
siTBC1D2 B
siTBC1D2 C
Area of GFP-LC3 puncta (A.U.)
2500
2000
600
400
200
0
-CQ
+CQ
E
MII-GFP-LC3
siCo.
siYAP/TAZ
siTBC1D2
- CQ
+ CQ
Empty
Flag-YAP WT
GFP-LC3/Flag/DAPI
a
b
c
d
e
f
F
siCo.
siYAP/TAZ
siTBC1D2
Area of GFP-LC3 puncta (A.U.)
1500
1000
250
200
150
100
50
0
1 2 3 4 5 6 7 8 9 10 11 12
Empty
YAP WT
Empty
YAP WT
-CQ
+CQ

Figure 6

Figure 7 YAP/TAZ require autophagy to sustain oncogenic traits and CSC properties.

(A) Representative images of MDA-MB-231 in clonogenic assays. For siRNA transfection conditions, MDA-MB-231 were transfected with control siRNA (siCo.), three TBC1D2 siRNAs (siTBC1D2 A, siTBC1D2 B and siTBC1D2 C), ATG7 siRNA (siATG7) or YAP/TAZ siRNAs (siYAP/TAZ). After 24 hours, cells were replated to clonogenic density. For pharmacological inhibition of autophagy, MDA-MB-231 were plated to clonogenic density and treated with vehicle or with two independent autophagy inhibitors (CQ: chloroquine 25μM; 3-MA: 3-methyladenine 10μM). 7 days after plating, cells were fixed and stained with crystal violet solution.

(B) Quantification of colony formation in MDA-MB-231 cells treated as in (A). Data were analyzed from three independent experiments. Bars represent mean + SEM (*$P<0.0001$ compared to siCo; §$P<0.0001$ compared to Vehicle; one-way ANOVA).

(C) Representative images of MDA-MB-231 in soft-agar assays. For siRNA transfection conditions, MDA-MB-231 were transfected with control siRNA (siCo.), three TBC1D2 siRNAs (siTBC1D2 A, siTBC1D2 B and siTBC1D2 C), ATG7 siRNA (siATG7) or YAP/TAZ siRNAs (siYAP/TAZ). After 24 hours, cells were replated in soft-agar condition. For pharmacological inhibition of autophagy, MDA-MB-231 were plated in soft-agar condition and treated with vehicle or with two independent autophagy inhibitors (CQ: 25μM; 3-MA: 10μM). 20 days after plating, cells were fixed with 4% PFA analyzed for the anchorage-independent growth in soft-agar. Scale bar: 200μm.

(D) Quantification of soft-agar growth in MDA-MB-231 cells treated as in (C). Data were analyzed from three independent experiments. Bars represent mean + SEM (*$P<0.0001$ compared to siCo; §$P<0.0001$ compared to Vehicle; one-way ANOVA).

(E) Representative images of MII mammosphere assays. MII cells overexpressing the TAZ S89A-construct were transfected with control siRNA (siCo.), three TBC1D2 siRNAs (siTBC1D2 A, siTBC1D2 B and siTBC1D2 C) or ATG7 siRNA (siATG7). After 24 hours, cells were replated on low attachment surface in mammosphere-forming medium. Alternatively, MII-TAZ S89A cells were plated

on ultralow attachment surface in mammosphere-forming medium and treated with vehicle or with two independent autophagy inhibitors (CQ, 25µM; 3-MA: 10µM). MII cells transduced with an empty vector (Empty) were used as negative control. Images were acquired 5 days after plating. Scale bar: 100µm.

(F) Quantification of mammosphere formation according to (E). Data were analyzed from three independent experiments. Bars represent mean + SEM (*P<0.0001 compared to siCo; §P<0.0001 compared to Vehicle; one-way ANOVA).

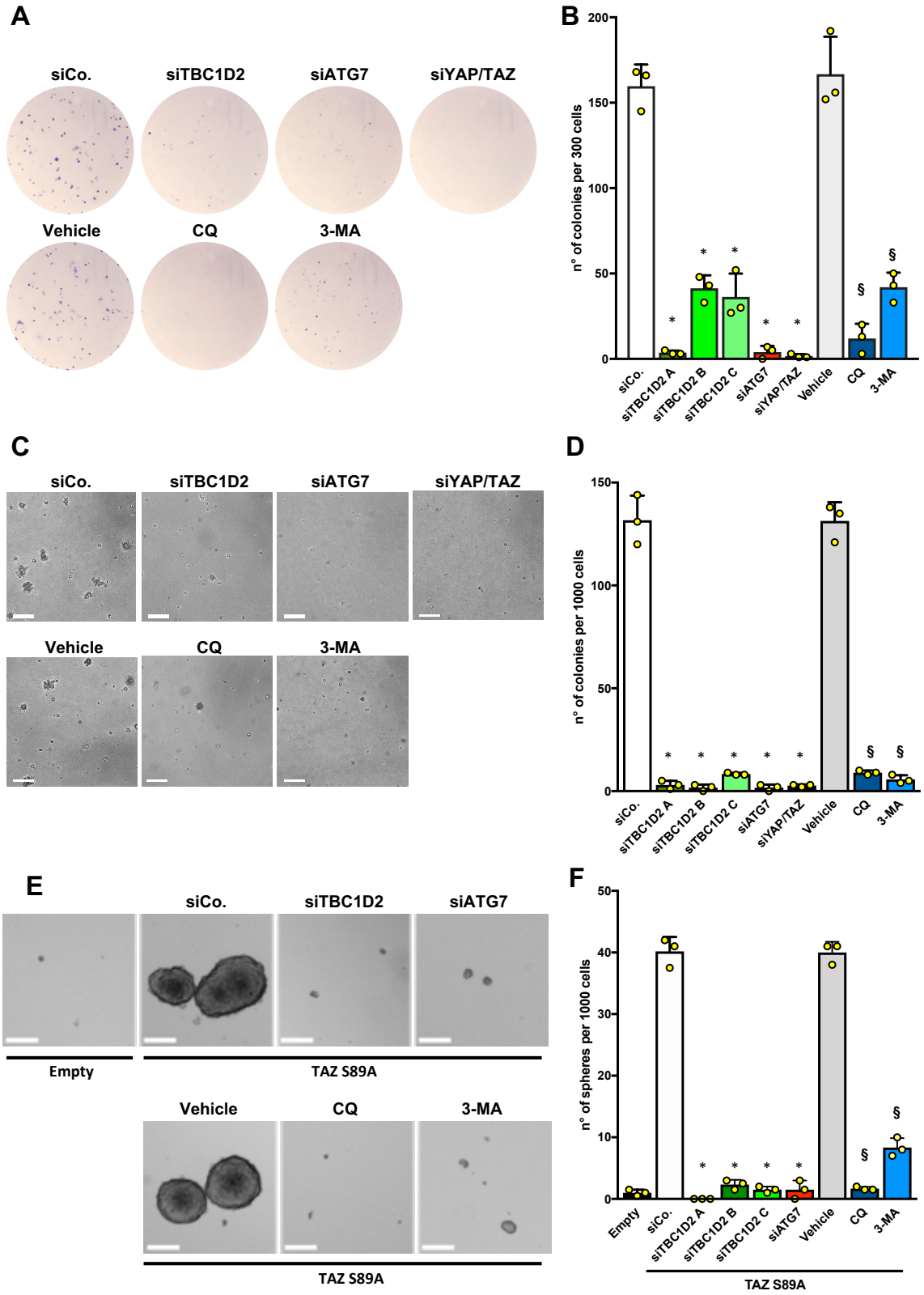
A
siCo.
siTBC1D2
siATG7
siYAP/TAZ
Vehicle
CQ
3-MA
B
n° of colonies per 300 cells
200
150
100
50
0
siCo.
siTBC1D2 A
siTBC1D2 B
siTBC1D2 C
siATG7
siYAP/TAZ
Vehicle
CQ
3-MA
C
siCo.
siTBC1D2
siATG7
siYAP/TAZ
Vehicle
CQ
3-MA
D
n° of colonies per 1000 cells
150
100
50
0
siCo.
siTBC1D2 A
siTBC1D2 B
siTBC1D2 C
siATG7
siYAP/TAZ
Vehicle
CQ
3-MA
E
siCo.
siTBC1D2
siATG7
Empty
TAZ S89A
Vehicle
CQ
3-MA
TAZ S89A
F
n° of spheres per 1000 cells
50
40
30
20
10
0
Empty
siCo.
siTBC1D2 A
siTBC1D2 B
siTBC1D2 C
siATG7
Vehicle
CQ
3-MA
TAZ S89A

Figure 7

Figure 8 YAP/TAZ require autophagy to reprogram mammary luminal differentiated cells into MaSC-like cells and sustain their self-renewal ability.

(A) Schematic of the experiments performed with luminal differentiated (LD) cells. LD cells were isolated through FACS sorting from dissociated mammary gland, plated on collagen I-coated supports and transduced with rtTA-encoding lentiviruses in combination with an empty vector or a doxycycline-inducible lentiviral YAP construct. After infection, cells were treated with 2μg/ml doxycycline to induce YAP expression, and either vehicle or 10μM 3-MA. After 7 days, cells were replated in MG colony medium with the indicated treatments and growth as mammary colonies

(B) Representative images of mammary colonies formed by the indicated cells 15 days after seeding in MG colony medium. Scale bars, 20μm.

(C) Quantifications of mammary colonies treated as in (A-B). Data were analyzed from two independent experiments with two technical replicates each. Bars represent mean + SEM (*P<0.0001 compared to Vehicle; one-way ANOVA).

(D-E) Autophagy inhibition impairs yMaSCs self-renewal ability. (D) Representative images of yMaSCs obtained from YAP-dependent reprogramming of LD cells, cultured in MG colony medium and treated with either vehicle or two independent autophagy inhibitors (CQ, 25μM; 3-MA: 10μM). Images were acquired 12 days after plating. Scale bars, 20μm. (E) Quantification of mammary colonies treated as in (D). Data were analyzed from three independent experiments. Bars represent mean + SEM (*P<0.0001 compared to Vehicle; one-way ANOVA).

(F-G) Autophagy inhibition impairs yMaSCs ability to grow as organoids. (F) Representative images of yMaSC grown for 12 days in organoid medium condition and treated with either empty vehicle or with two independent autophagy inhibitors (CQ, 25μM; 3-MA: 10μM). Scale bars, 50μm. (G) Quantification of mammary organoids obtained from yMaSC according to (F). Data were analyzed from two independent experiments with three technical replicates each. Bars represent mean + SEM (*P<0.0001 compared to Vehicle; one-way ANOVA).

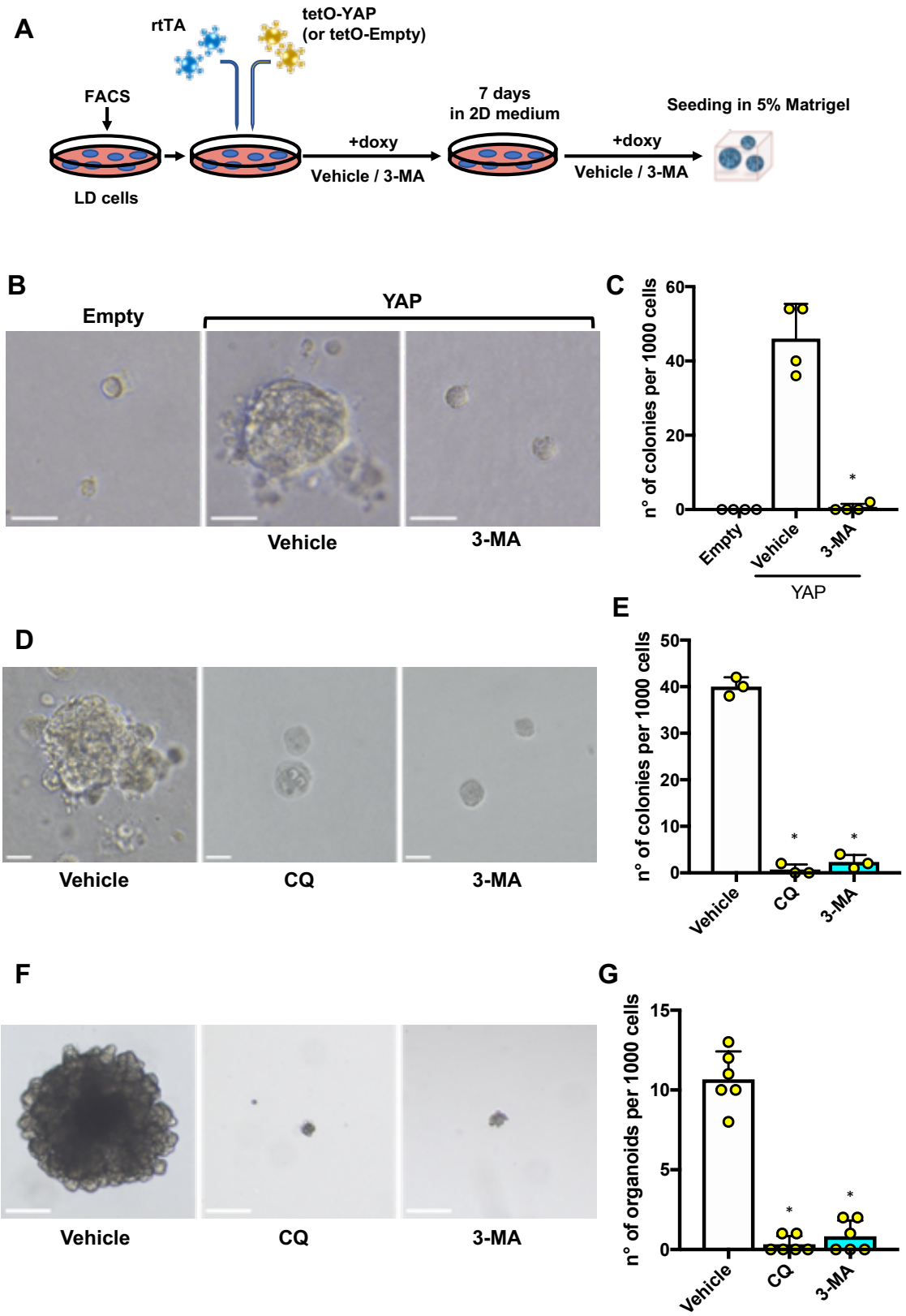
A
rtTA
tetO-YAP
(or tetO-Empty)
FACS
LD cells
+doxy
Vehicle / 3-MA
7 days
in 2D medium
+doxy
Vehicle / 3-MA
Seeding in 5% Matrigel
B
Empty
YAP
Vehicle
3-MA
C
n° of colonies per 1000 cells
60
40
20
0
Empty
Vehicle
3-MA
YAP
D
Vehicle
CQ
3-MA
E
n° of colonies per 1000 cells
50
40
30
20
10
0
Vehicle
CQ
3-MA
F
Vehicle
CQ
3-MA
G
n° of organoids per 1000 cells
15
10
5
0
Vehicle
CQ
3-MA

Figure 8

Figure 9 YAP/TAZ require autophagy to reprogram exocrine cells into pancreatic progenitors and sustain their self-renewal abilities.

(A) Immunoblot analysis for LC3 protein of lysates obtained from acinar cells (acini) and YAP-induced pancreatic organoids (yDuct) cultured with normal medium (-CQ) or with 50μM CQ (+CQ) for 4 hours. The cleaved LC3 peptide and its phosphatidylethanolamine conjugated form are indicated as LC3-I and LC3-II respectively. GAPDH serves as loading control.
(B) Schematic of the experiments performed with pancreatic acinar explants. Pancreatic acini dissociated from *R26-rtTA; tetO-YAP*^{S127A} mice were seeded in collagen-I based hydrogels and cultured in the presence of 2μg/ml doxycycline (doxy), to induce the expression of the transgenic YAP, and either vehicle or two independent autophagy inhibitors CQ (25μM) or 3-MA (10μM). Acinar cells were cultured for 5 days in the described condition and analyzed for the appearance of yDucts structures. Pancreatic acini cultured without doxycycline (-doxy) were used as negative control of cell programming.
(C-D) Representative images (C) and quantification (D) of yDuct structures obtained upon YAP-dependent reprogramming of acinar cells treated as in (B). Scale bars, 50μm (C). Data were analyzed from two independent experiments. Bars represent mean + SEM (*P<0.001 compared to Vehicle; one-way ANOVA) (D).
(E-F) Autophagy inhibition impairs self-renewal ability of yDucts. (E) Representative images of yDucts replated at the single cell level in organoid condition with empty vehicle or with two independent autophagy inhibitors (CQ, 25μM; 3-MA: 10μM). Images were acquired 12 days after seeding. Scale bars, 20μm. (F) Quantification of yDuct organoids according to (E). Data were analyzed from two independent experiments. Bars represent mean + SEM (*P<0.01 compared to Vehicle; one-way ANOVA).

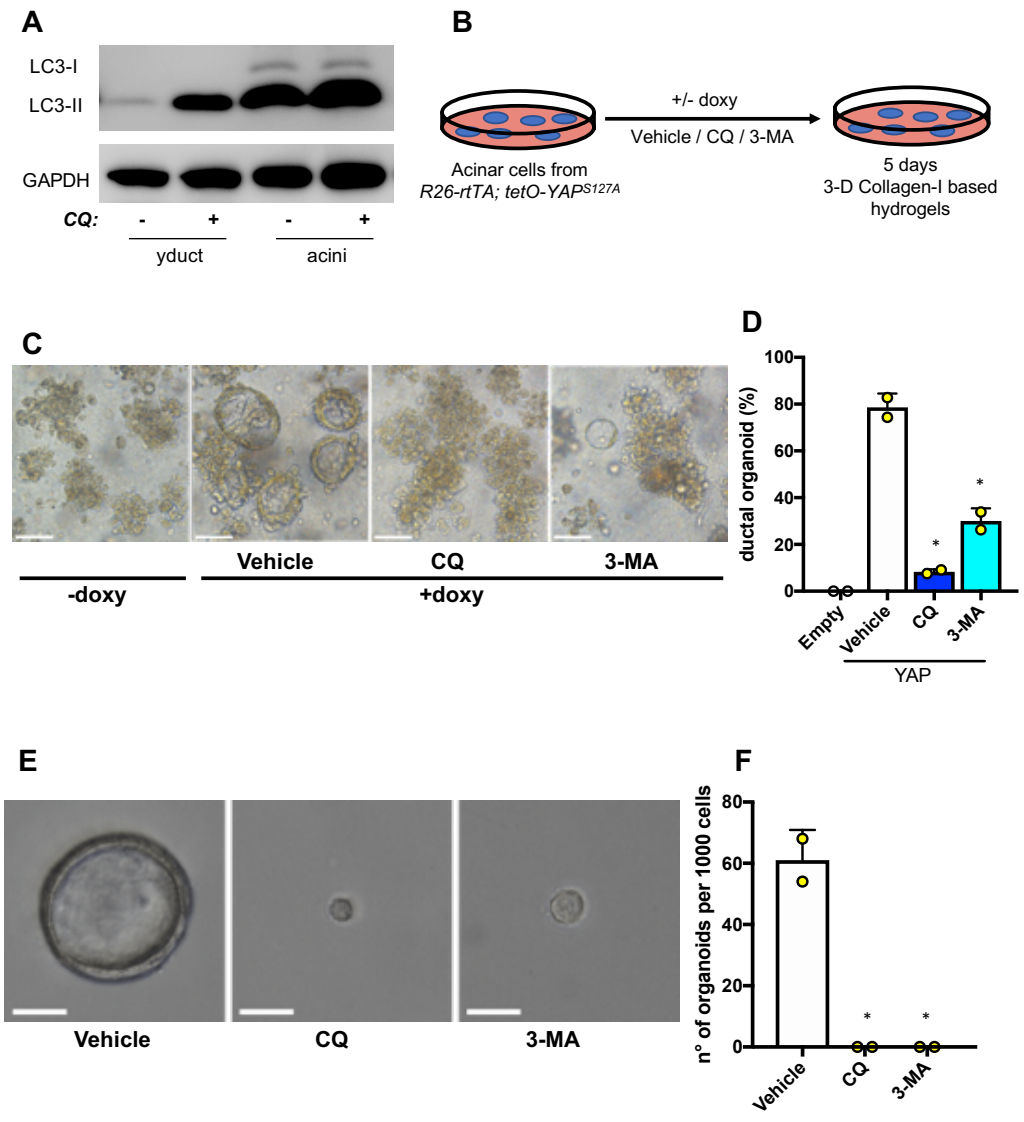
A
LC3-I
LC3-II
GAPDH
CQ: - + - +
yduct
acini
B
+/- doxy
Vehicle / CQ / 3-MA
Acinar cells from
R26-rtTA; tetO-YAP S127A
5 days
3-D Collagen-I based
hydrogels
C
Vehicle
CQ
3-MA
-doxy
+doxy
D
ductal organoid (%)
100
80
60
40
20
0
Empty
Vehicle
CQ
3-MA
YAP
E
Vehicle
CQ
3-MA
F
n° of organoids per 1000 cells
80
60
40
20
0
Vehicle
CQ
3-MA

Figure 9